



A material/element-defined time integration procedure for dynamic analysis

Delfim Soares Jr.¹

Received: 23 November 2022 / Accepted: 12 July 2023 / Published online: 14 August 2023
© The Author(s), under exclusive licence to Springer-Verlag London Ltd., part of Springer Nature 2023

Abstract

In this paper, an effective and highly versatile locally-defined time-marching procedure is proposed for dynamic analysis. In this novel technique, the time integration parameters of the method are specified at an element level, adapting themselves to the features of the adopted discretization and to the local properties of the model. In this sense, the errors of the co-applied spatial discretization method may be properly counterbalanced by the calculations of the proposed time integration procedure, providing considerably more accurate results. Controllable numerical dissipation is also enabled by the novel approach, allowing the user to determine the regions of the model in which algorithmic damping is to be applied, as well as to define its intensity. Consequently, in the proposed formulation, an additional “material” parameter may be inputted for the analysis (similarly to those defining the physical properties of the model), delineating the numerical features of the considered solution procedure to be locally applied. The proposed formulation is highly accurate, efficient, and simple to implement. It also provides guaranteed stability and improved dissipative analyses, standing as a very effective time-marching technique. At the end of the paper, numerical results are presented and compared to those of standard formulations, illustrating the enhanced performance of the proposed novel procedure.

Keywords Time integration · Locally-defined parameters · Adaptive analysis · Controllable numerical dissipation · Enhanced accuracy · Wave propagation models

1 Introduction

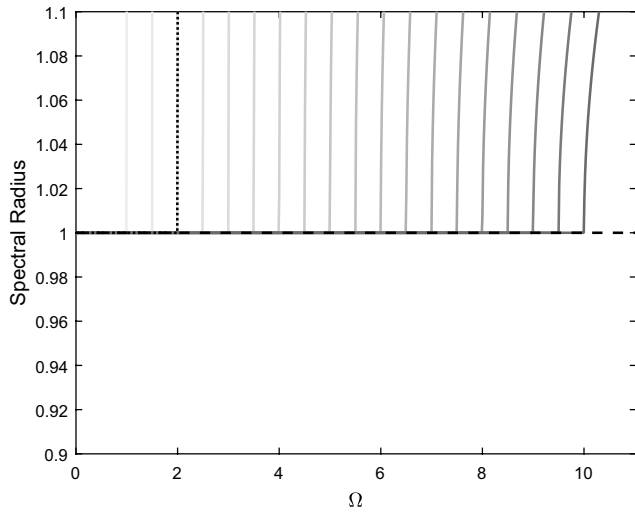
In order to find a solution for governing differential equations describing complex real-world transient models, one has to employ spatial and temporal discretization methods. In this sense, separation of space and time domains is usually employed, and spatial discretization procedures are typically first considered, leading to a time-domain semi-discrete system of equations, which is then analysed by a time integration procedure. The Finite Element Method (FEM) [1, 2], as well as many other formulations based on local approximations, has been successfully employed in engineering practice and in many other fields of industry and science to solve problems based on partial differential equations. In fact, local approaches are widely explored in what spatial discretization is concerned; however, this is not

the case for problems in which time integration is regarded. In this context, local approximations are mostly based on a temporal and/or spatial definition of the time-step value (i.e., the development of adaptive time stepping techniques [3–7] and/or multi-time-steps/sub-cycling splitting procedures [8–12]). However, much more can be explored in this field.

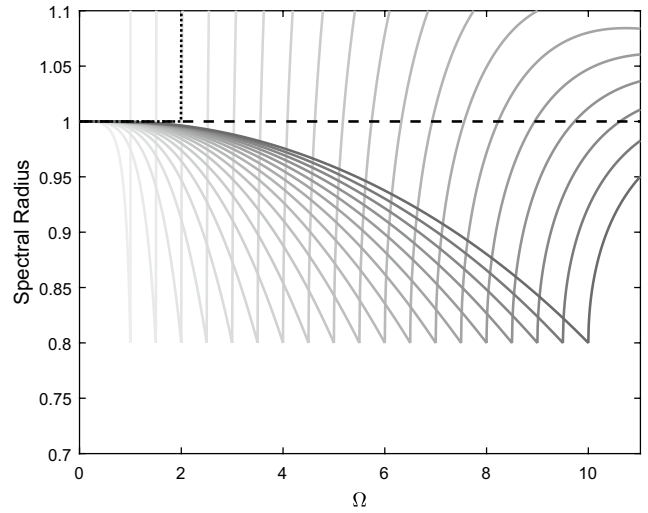
In this work, a novel locally-defined time integration procedure is proposed, aiming to provide a highly versatile and effective time-domain formulation for dynamic analyses. The proposed technique is based on locally computed time integration parameters, which self-adjust to the properties of the spatially-temporally discretized model and to a user-defined input parameter, which allows introducing different numerical features for different subdomains of the model. In this context, (i) a link between the adopted spatial and temporal discretization procedures is established, allowing their errors to be better counterbalanced and enhanced accuracy provided; (ii) specific numerical characteristics, such as algorithmic damping, may be locally applied as one wishes (e.g., considering predefined regions, different intensities etc.), further improving the accuracy of the proposed

✉ Delfim Soares Jr.
delfim.soares@ufjf.edu.br

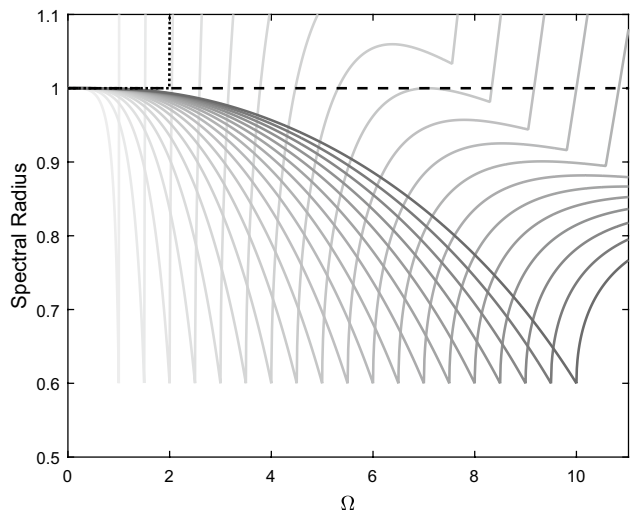
¹ Structural Engineering Department, Federal University of Juiz de Fora, Juiz de Fora, MG 36036-330, Brazil



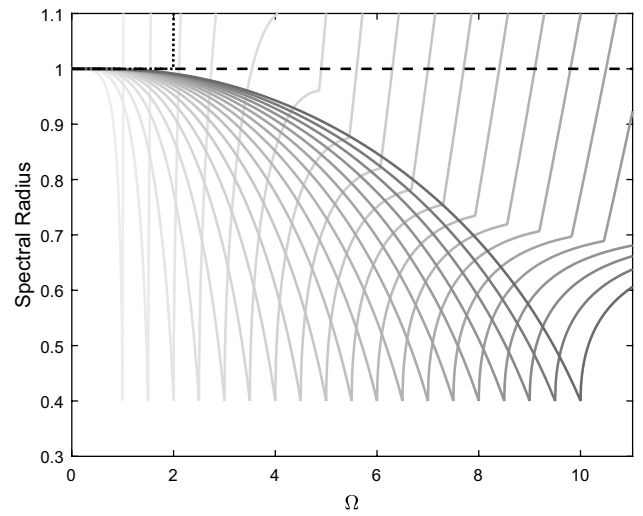
(a)



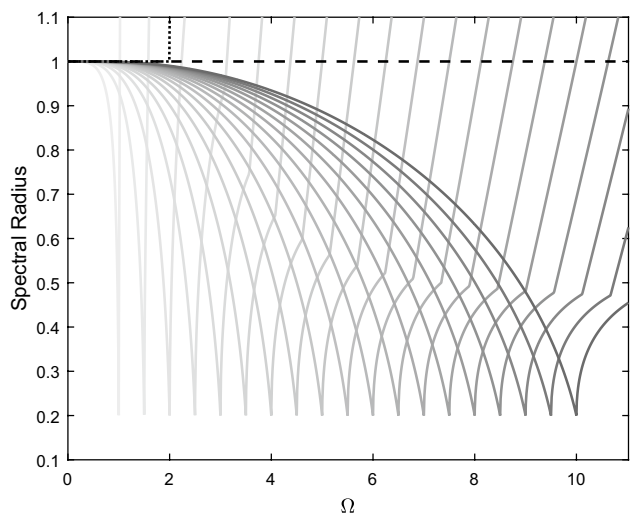
(b)



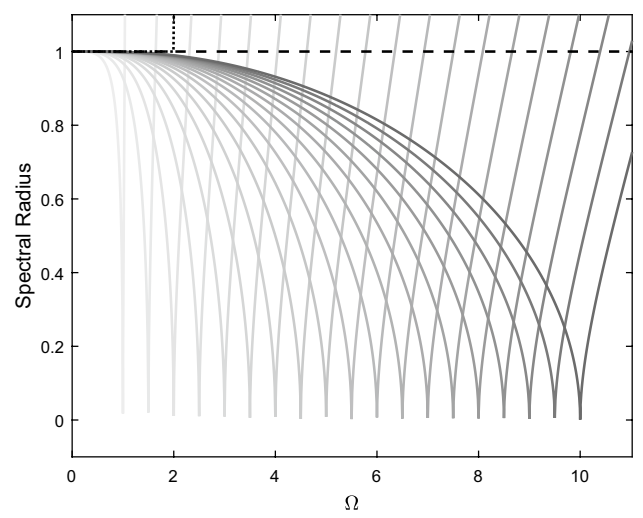
(c)



(d)



(e)



(f)

Fig. 1 Spectral radii for $\Omega_b=1, 1.5, \dots, 10$ (lighter to darker gray color), considering the new methodology with different ρ_b^0 values (for $\xi=0.0$): **a** 1.0; **b** 0.8; **c** 0.6; **d** 0.4; **e** 0.2; **f** 0.0. Results for the CD and the TR are depicted as black dotted and dashed lines, respectively, for reference. (Color figure online)

solution procedure, as well as its flexibility; (iii) hybrid numerical analyses may be easily carried out, avoiding complex subdomain/interface definitions and/or treatments.

In fact, in the proposed technique, an additional “material” parameter, similarly to those defined by the user to locally specify the physical properties of the model, may be inputted for the analysis, locally specifying the numerical properties of the applied solution procedure. In this work, this user-defined input parameter mainly controls the numerical dissipative features that are considered in the adopted solution process. Numerous efforts along the past few years have focused on developing both implicit [13–19] and explicit [20–27] time integration algorithms that include numerical dissipation of the high-frequency content, allowing to reduce spurious non-physical oscillations that sometimes occur due to the excitation of spatially unresolved modes. Nevertheless, designing such algorithms may be challenging as one should add proper high-frequency dissipation without introducing excessive algorithmic damping into the important low frequency modes. In this case, since the proposed time integration procedure allows highly flexible configurations, it may better deal with this dilemma than standard procedures, establishing more appropriate solution strategies for effective dissipative analyses. Additionally, since the proposed technique adapts to the properties of the problem, it enables properly “tracking” the higher-frequency range of the model, enhancing the performance of its dissipative computations.

A locally-defined strategy, in which a new “material” parameter is inputted to locally specify the features of the applied numerical solution procedure, has already been reported taking into account structural dynamic models [28], providing good responses. However, in the present work, this idea is much deeply explored and novel recurrence relations and time integration parameters are formulated, allowing to develop a considerably more effective solution procedure. In this context, the presently proposed technique considers some concepts that have been alternatively forged for explicit time-marching techniques [29, 30], enabling enhanced adaptive computations to be carried out for both dissipative and non-dissipative analyses. Nonetheless, oppositely to what is requested by explicit approaches, the adopted time-step of the discussed time-marching procedure does not need to be equal to or lower than a critical time-step value to provide stable analyses, since guaranteed stability is ascertained by the novel methodology. In fact, as it is discussed along this paper, several other additional positive features are enabled

by the proposed new technique, describing a very promising time integration procedure.

The proposed formulation is based on a simple, single-step, truly self-starting, time-marching framework, which was proposed by the author [31] and has been extensively explored along the last decade providing several highly effective explicit [24, 32] and extended-explicit [25, 29, 30] solution procedures, as well as very versatile explicit-explicit [12, 33] and explicit-implicit approaches [34, 35]. Notwithstanding, as in [28], this paper focuses on developing an implicit time-marching technique that is highly accurate and considers just one solver procedure per time step (in opposite to composite approaches [15, 17, 18]), describing an efficient formulation for implicit analyses.

The manuscript is organized as follows: first, the governing equations of the model and the proposed locally-defined time integration procedure are presented, describing the basic aspects of the novel solution methodology; in the sequence, the properties of the method are discussed, and numerical applications are provided, illustrating the great effectiveness of the proposed formulation; finally, at the end of the paper, conclusions are presented, summarizing the several positive features of the novel technique.

2 Locally-defined time integration procedure

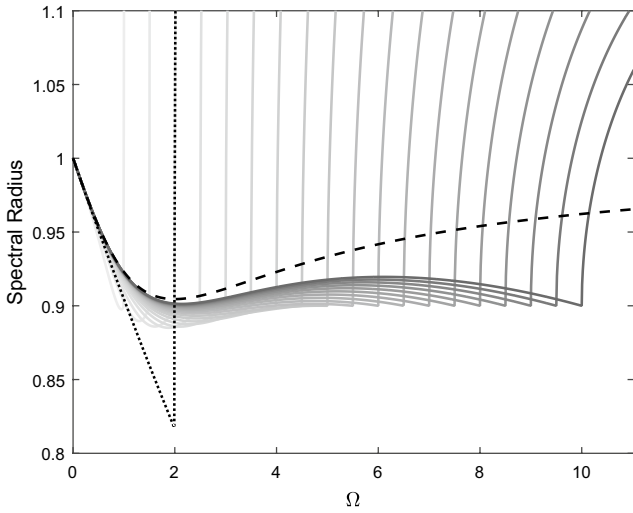
Governing equations that describe wave propagation models, as well as many other physical problems, require both spatial and temporal discretization procedures to be conjointly applied, so that they can be properly numerically treated. In this sense, spatial discretization techniques are usually first considered, providing a time-domain semi-discrete system of equations that may be generically written as [1]:

$$M\ddot{U}(t) + C\dot{U}(t) + KU(t) = F(t) \tag{1}$$

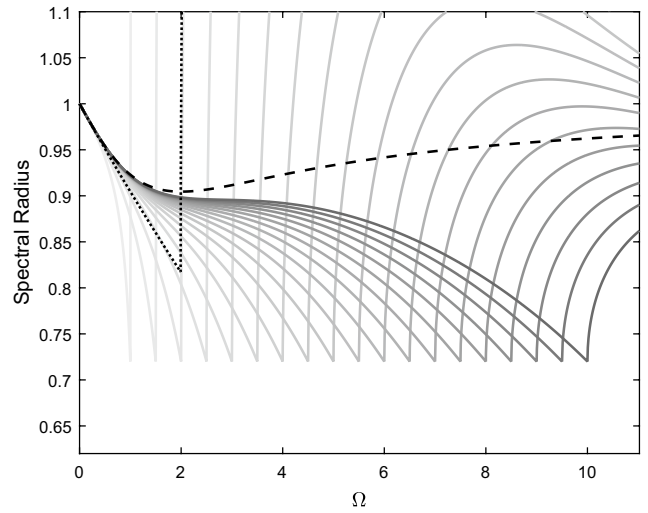
Table 1 Solution algorithm for each time step of the analysis

1. Compute vector \bar{F} by time integrating the force vector:

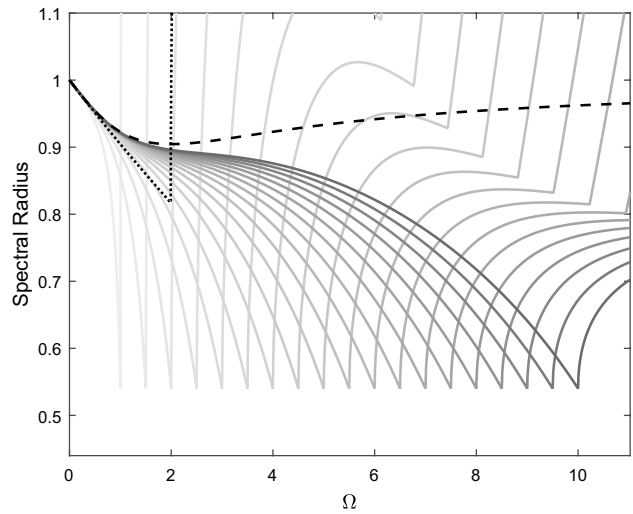
$$\bar{F} = \int_{t^n}^{t^{n+1}} F(\tau) d\tau;$$
2. Compute vector Λ :
 - 2.1 Initialize vector $V = 0$ and, for each element e of the spatial discretization: If $(\mu_1^e \neq 0$ or $\mu_2^e \neq 0)$, assemble $K_e(\mu_1^e U_e^n + \mu_2^e \Delta t \dot{U}_e^n)$ into V ;
 - 2.2. Compute: $\Lambda = M^{-1} V$;
3. Compute the velocity vector:
 - 3.1. Solve: $E\Delta\dot{U} = \bar{F} - \Delta t [C\dot{U}^n + K(U^n + \frac{1}{2}\Delta t \dot{U}^n + \Delta t^2 \Lambda)]$; (where E is defined by the assembling of $M_e + \frac{1}{2}\Delta t C_e + \mu_0^e \Delta t^2 K_e$)
 - 3.2. Compute: $\dot{U}^{n+1} = \dot{U}^n + \Delta\dot{U}$;
4. Compute the displacement vector: $U^{n+1} = U^n + \frac{1}{2}\Delta t(\dot{U}^n + \dot{U}^{n+1})$;



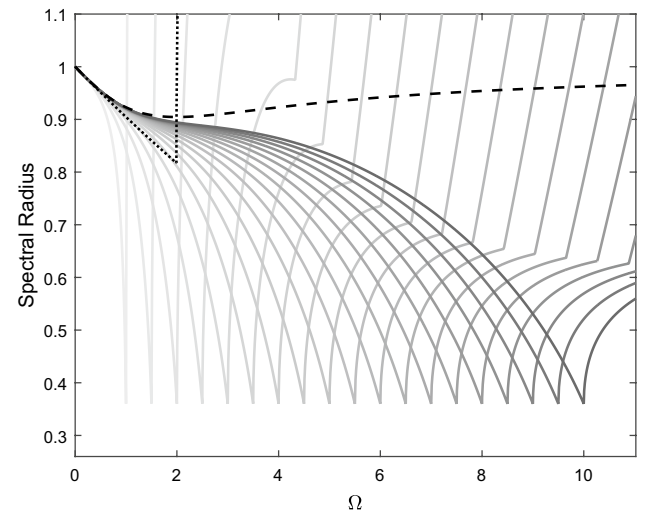
(a)



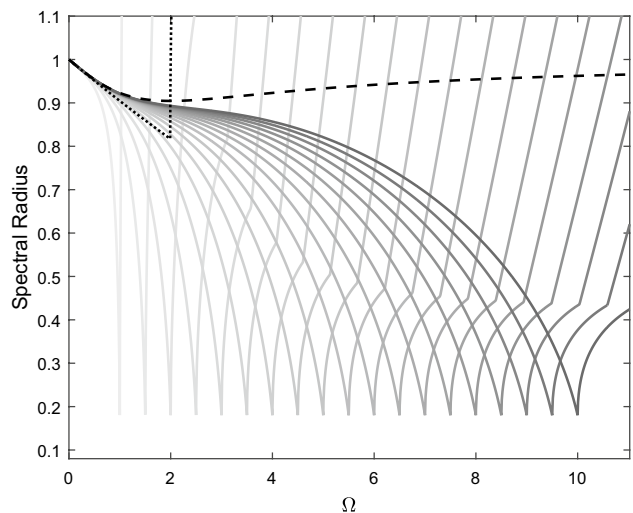
(b)



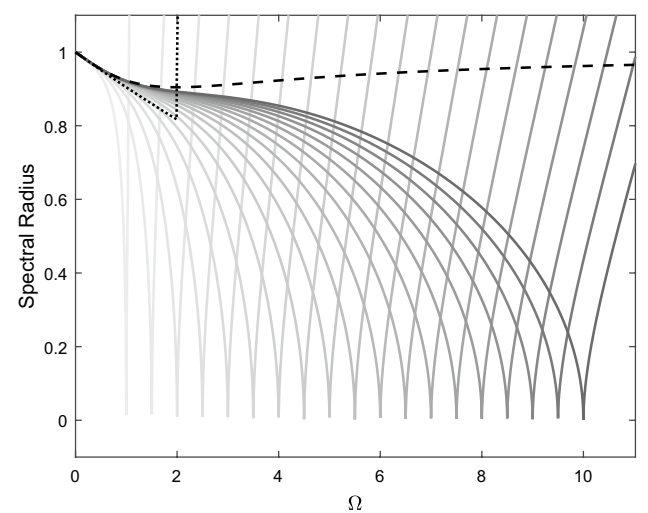
(c)



(d)



(e)



(f)

Fig. 2 Spectral radii for $\Omega_b=1, 1.5, \dots, 10$ (lighter to darker gray color), considering the new methodology with different ρ_b^0 values (for $\xi=0.1$): **a** 1.0; **b** 0.8; **c** 0.6; **d** 0.4; **e** 0.2; **f** 0.0. Results for the CD and the TR are depicted as black dotted and dashed lines, respectively, for reference. (Color figure online)

where, by adopting a solid mechanics nomenclature, \mathbf{M} , \mathbf{C} and \mathbf{K} stand for the mass, damping and stiffness matrices of the spatially discretized model, respectively, $\mathbf{F}(t)$ stands for its force vector, and $\mathbf{U}(t)$, $\dot{\mathbf{U}}(t)$ and $\ddot{\mathbf{U}}(t)$ represent displacement, velocity and acceleration vectors, respectively. The initial conditions of this hyperbolic problem are given by $\mathbf{U}^0 = \mathbf{U}(0)$ and $\dot{\mathbf{U}}^0 = \dot{\mathbf{U}}(0)$, where \mathbf{U}^0 and $\dot{\mathbf{U}}^0$ stand for initial displacement and velocity vectors, respectively.

By time integrating Eq. (1), considering a time-step Δt (i.e., $t^{n+1} = t^n + \Delta t$), the following expression may be established:

$$\mathbf{M} \int_{t^n}^{t^{n+1}} \ddot{\mathbf{U}}(t)dt + \mathbf{C} \int_{t^n}^{t^{n+1}} \dot{\mathbf{U}}(t)dt + \mathbf{K} \int_{t^n}^{t^{n+1}} \mathbf{U}(t)dt = \int_{t^n}^{t^{n+1}} \mathbf{F}(t)dt \tag{2}$$

where the integrals on its left-hand-side may be defined as:

$$\int_{t^n}^{t^{n+1}} \ddot{\mathbf{U}}(t)dt = \dot{\mathbf{U}}^{n+1} - \dot{\mathbf{U}}^n \tag{3a}$$

$$\int_{t^n}^{t^{n+1}} \dot{\mathbf{U}}(t)dt = \mathbf{U}^{n+1} - \mathbf{U}^n \tag{3b}$$

$$\int_{t^n}^{t^{n+1}} \mathbf{U}(t)dt = \Delta t \mathbf{U}^n + \left(\frac{1}{2} - \mu_0\right) \Delta t^2 \dot{\mathbf{U}}^n + \mu_0 \Delta t^2 \dot{\mathbf{U}}^{n+1} \tag{3c}$$

in which \mathbf{U}^n and $\dot{\mathbf{U}}^n$ represent the approximations of $\mathbf{U}(t^n)$ and $\dot{\mathbf{U}}(t^n)$, respectively, and μ_0 stands for a time integration parameter for the proposed solution methodology.

By considering Eqs. (3a, 3b, 3c), as well as a simple finite difference expression to define the current displacement vector (see Eq. (4b)), Eq. (2) may be rewritten, allowing to establish Eq. (4a):

$$\left(\mathbf{M} + \frac{1}{2} \Delta t \mathbf{C} + \mu_0 \Delta t^2 \mathbf{K}\right) \dot{\mathbf{U}}^{n+1} = \bar{\mathbf{F}} + \mathbf{M} \dot{\mathbf{U}}^n - \frac{1}{2} \Delta t \mathbf{C} \dot{\mathbf{U}}^n - \Delta t \mathbf{K}(\mathbf{U}^n + \left(\frac{1}{2} - \mu_0\right) \Delta t \dot{\mathbf{U}}^n) \tag{4a}$$

$$\mathbf{U}^{n+1} = \mathbf{U}^n + \frac{1}{2} \Delta t (\dot{\mathbf{U}}^n + \dot{\mathbf{U}}^{n+1}) \tag{4b}$$

In this equation, $\bar{\mathbf{F}}$ stands for the time integral of the force term (as indicated on the right-hand-side of Eq. (2)), which can be analytically evaluated or numerically computed considering any standard formulation to evaluate the numerical value of a definite integral (e.g., the rectangular rule: $\bar{\mathbf{F}} = \Delta t \mathbf{F}^{n+\eta}$, were $0 \leq \eta \leq 1$; the trapezoidal rule: $\bar{\mathbf{F}} = \frac{1}{2} \Delta t \mathbf{F}^n + \frac{1}{2} \Delta t \mathbf{F}^{n+1}$; etc.).

As one may observe, Eqs. (4a) and (4b) allow to compute of the velocities and displacements of the model, respectively, at the current time step of the analysis. The solution algorithm described by these equations may be regarded as a particular configuration of the more generic time-marching solution procedure proposed by Soares [31] and, as so, it describes a simple, truly self-starting, single-step, non-dissipative formulation, which becomes spectrally equivalent to the Central Difference (CD) method for $\mu_0 = 0$, and reproduces the Trapezoidal Rule (TR) for $\mu_0 = 1/4$.

In this work, this solution procedure is modified, and new recurrence relationships are proposed, allowing to introduce numerical dissipation into the analysis, as well as to enhance the accuracy and versatility of the developed technique. In this context, the solution algorithm described by Eqs. (4a, 4b) may be reformulated, introducing an auxiliary vector $\mathbf{\Lambda}$ into the methodology and rewriting Eq. (4a) in a more suitable configuration, as indicated next:

$$\mathbf{M} \mathbf{\Lambda} = \mathbf{K}(\mu_1 \mathbf{U}^n + \mu_2 \Delta t \dot{\mathbf{U}}^n) \tag{5a}$$

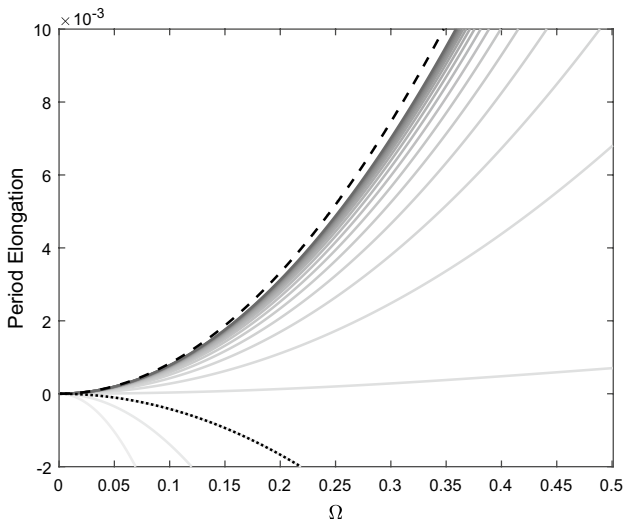
$$\left(\mathbf{M} + \frac{1}{2} \Delta t \mathbf{C} + \mu_0 \Delta t^2 \mathbf{K}\right) \Delta \dot{\mathbf{U}} = \bar{\mathbf{F}} - \Delta t [\mathbf{C} \dot{\mathbf{U}}^n + \mathbf{K}(\mathbf{U}^n + \frac{1}{2} \Delta t \dot{\mathbf{U}}^n + \Delta t^2 \mathbf{\Lambda})] \tag{5b}$$

$$\dot{\mathbf{U}}^{n+1} = \dot{\mathbf{U}}^n + \Delta \dot{\mathbf{U}} \tag{5c}$$

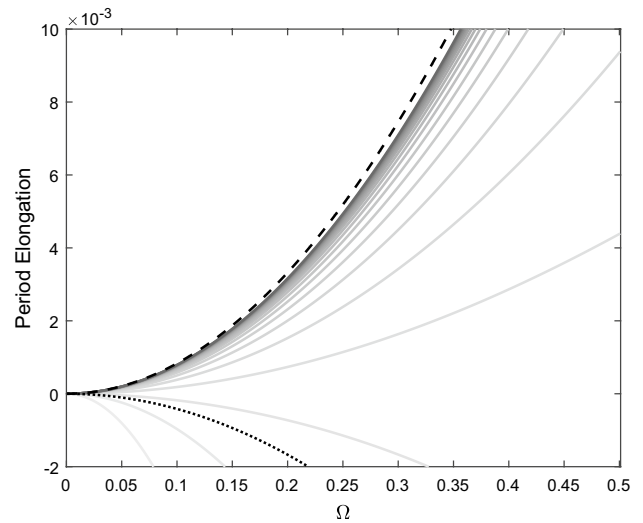
$$\mathbf{U}^{n+1} = \mathbf{U}^n + \frac{1}{2} \Delta t (\dot{\mathbf{U}}^n + \dot{\mathbf{U}}^{n+1}) \tag{5d}$$

In this novel solution procedure, $\mathbf{\Lambda}$ stands for a numerical (i.e., non-physical) acceleration vector, which is established considering the time integration parameters μ_1 and μ_2 . These parameters control the numerical dissipative features of the novel approach and, for $\mu_1 = \mu_2 = 0$, numerical dissipation is not introduced into the analysis (in this case, Eqs. (5a, 5b, 5c, 5d) reproduce the methodology described by Eqs. (4a, 4b)).

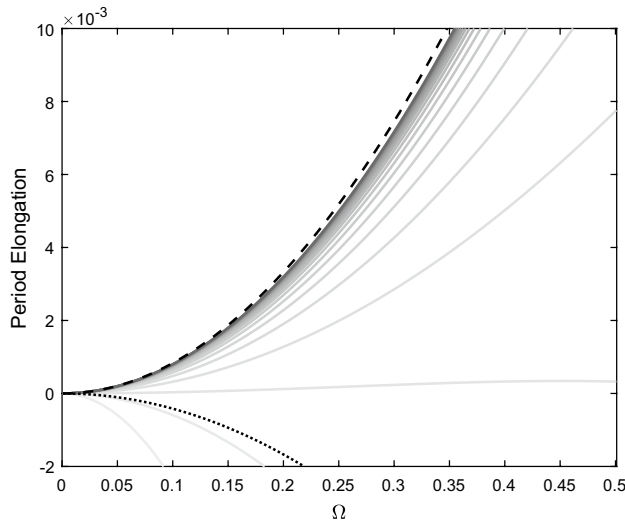
Equations (5a, 5b, 5c, 5d) delineate the proposed time-marching procedure. As previously remarked, this formulation stands as a single-step methodology based only on velocities and displacements, being no computation of physical accelerations necessary (of course, if required, these accelerations may be post-processed, considering any proper numerical procedure). Thus, the proposed technique stands as a truly self-starting approach, eliminating any kind of cumbersome initial calculation. Moreover, as it may be observed, if lumped mass matrices are considered (as it is carried out in this work), just one system of equations has to be dealt with following the proposed formulation (i.e., the one described in Eq. (5b)) and, in this case, the technique also stands as a single-solver procedure, avoiding excessive computational efforts, which are



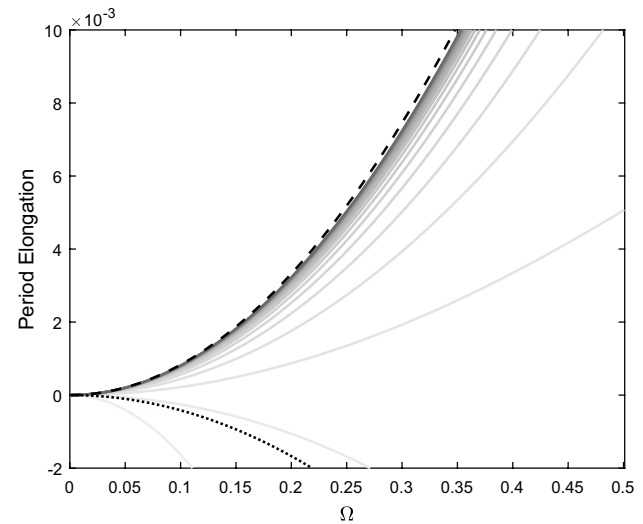
(a)



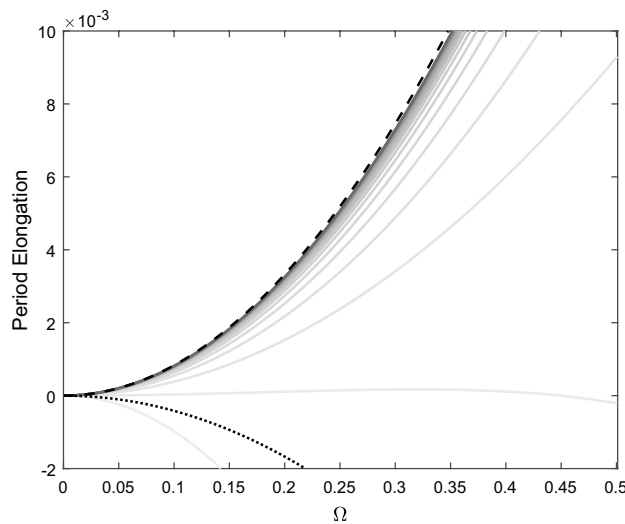
(b)



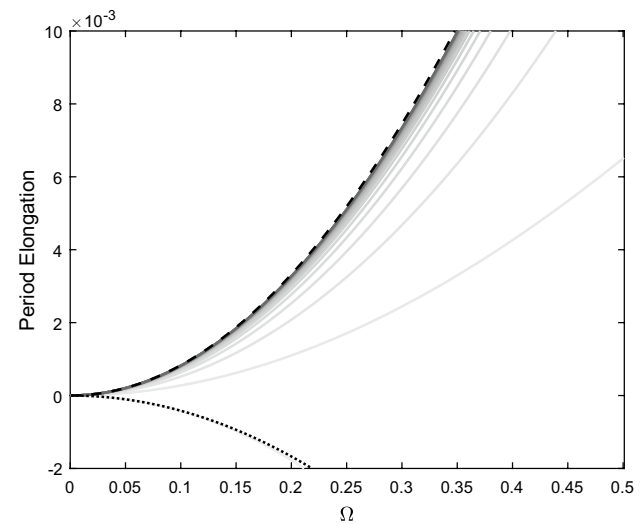
(c)



(d)



(e)



(f)

Fig. 3 Period elongation errors for $\Omega_b=1, 1.5, \dots, 10$ (lighter to darker gray color), considering the new methodology with different ρ_b^0 values: **a** 1.0; **b** 0.8; **c** 0.6; **d** 0.4; **e** 0.2; **f** 0.0. Results for the CD and the TR are depicted as black dotted and dashed lines, respectively, for reference. (Color figure online)

usual in composite time-marching formulations [15, 17, 18]. Additionally, the computational cost of the proposed technique may be further reduced if a locally defined formulation is regarded. In this context, Eq. (5a) may be rewritten as $\mathbf{M}\mathbf{\Lambda} = \mathbf{V}$, where vector \mathbf{V} is established taking into account the assembling of local vectors \mathbf{V}_e , which are evaluated for each element e of the adopted spatial discretization. In this case, \mathbf{V}_e may be computed as $\mathbf{K}_e(\mu_1^e \mathbf{U}_e^n + \mu_2^e \Delta t \dot{\mathbf{U}}_e^n)$ only if a so-called dissipative element is regarded (i.e., if $\mu_1^e \neq 0$ or $\mu_2^e \neq 0$), otherwise the referred element does not contribute to the reported assembling and \mathbf{V}_e does not need to be calculated, avoiding extra matrix–vector multiplications.

In fact, this locally-defined strategy may be much deeply explored and the three time integration parameters of the proposed technique may be locally configured, taking into account the properties of the discretized model to establish appropriate local values for μ_0 , μ_1 and μ_2 . In this context, not only a more efficient formulation may be provided (as previously discussed), but also a much more accurate solution methodology may be engendered, considering adaptive μ_0^e , μ_1^e and μ_2^e values. Thus, as reported, the above referred vector \mathbf{V} is here established considering the assembling of local vectors that are evaluated based on the values of μ_1^e and μ_2^e , and the effective matrix of the method (see the term in parenthesis on the left-hand-side of Eq. (5b)) is established taking into account the assembling of local matrices that are calculated based on the values of μ_0^e (i.e., the effective matrix is established by the assembling of $\mathbf{M}_e + \frac{1}{2} \Delta t \mathbf{C}_e + \mu_0^e \Delta t^2 \mathbf{K}_e$).

In this work, the elemental time integration parameters μ_0^e , μ_1^e and μ_2^e are defined as function of the maximal sampling frequency of the element Ω_e^{\max} (where $\Omega_e^{\max} = \omega_e^{\max} \Delta t$, and ω_e^{\max} stands for the highest natural frequency of the element, which is calculated based on its local matrices \mathbf{M}_e and \mathbf{K}_e) and of its damping ratio ξ_e (which is computed as $\xi_e = \zeta_e (2\rho_e \omega_e^{\max})^{-1}$, where ζ_e and ρ_e are the physical parameters of the model defining matrices \mathbf{C}_e and \mathbf{M}_e , respectively). Thus, μ_0^e , μ_1^e and μ_2^e are computed taking into account the local features of the spatially/temporally discretized model, establishing a link between the adopted spatial discretization method and the applied time integration approach, which

enables the errors of these procedures to be better counterbalanced. In this context, spatially-temporally computed solutions may become highly accurate, establishing a very effective time integration methodology.

The expressions that are here proposed to calculate the local time integration parameters μ_0^e , μ_1^e and μ_2^e are:

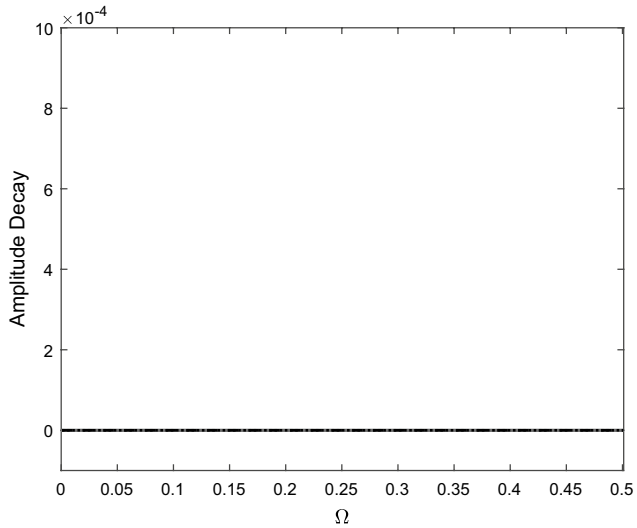
$$\mu_0^e = \frac{1}{4} - \Omega_e^{\max-2} \tag{6a}$$

$$\mu_1^e = \left\{ \left(\frac{1}{4} + \xi_e \Omega_e^{\max-1} \right) [\rho_b^0 (1 - \xi_e) + 1]^2 - 1 \right\} \Omega_e^{\max-2} \tag{6b}$$

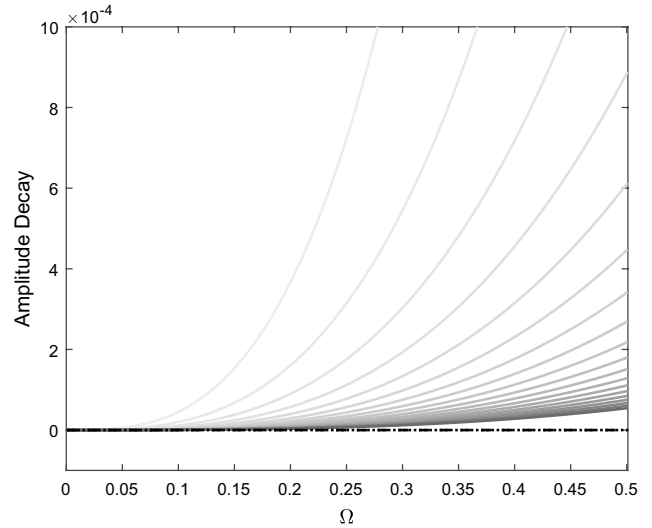
$$\mu_2^e = -\frac{1}{2} \left(\frac{1}{4} + \xi_e \Omega_e^{\max-1} \right) [\rho_b^0 (1 - \xi_e) - 1]^2 \Omega_e^{\max-2} \tag{6c}$$

where $0 \leq \rho_b^0 \leq 1$ stands as a input parameter (to be provided by the user, for different regions of the model), which controls the amount of numerical damping to be introduced into the analysis.

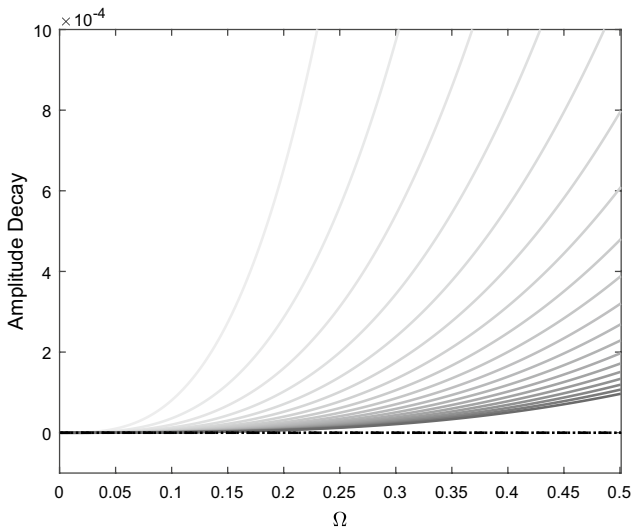
The developed expressions for μ_0^e , μ_1^e and μ_2^e (see Eqs. (6a, 6b, 6c)) are formulated to introduce maximal numerical damping at the maximal sampling frequency of the element e , so that the higher modes of the model may be effectively dissipated. In fact, by considering these expressions, the bifurcation spectral radius of the method becomes equal to $\rho_b^0 (1 - \xi_e)$ —thus, the input parameter ρ_b^0 represents the bifurcation spectral radius of the method for $\xi_e = 0$ (undamped model)—and its bifurcation sampling frequency becomes equal to the maximal sampling frequency of the focused element (i.e., $\rho_b \equiv \rho_b^0 (1 - \xi_e)$ and $\Omega_b \equiv \Omega_e^{\max}$). By following this design, maximal algorithmic damping is provided for Ω_e^{\max} (which enables a highly effective local dissipative procedure, allowing the influence of spurious high-frequency modes to be properly eliminated), and the intensity of this applied numerical dissipation is controlled by the input parameter ρ_b^0 , rendering a very flexible approach. Additionally, each element of the discretized model may consider a different ρ_b^0 value, so that numerical damping may be locally applied as one wishes, further improving the versatility of the proposed formulation. In this context, different ρ_b^0 values may be provided by the user for different regions of model, and ρ_b^0 may then be regarded as an additional “material” property to be specified in the analysis (such as the physical parameters defining matrices \mathbf{M} , \mathbf{C} and \mathbf{K} , for instance), controlling the amount of numerical dissipation to be locally applied. The purpose of numerical dissipation is to reduce



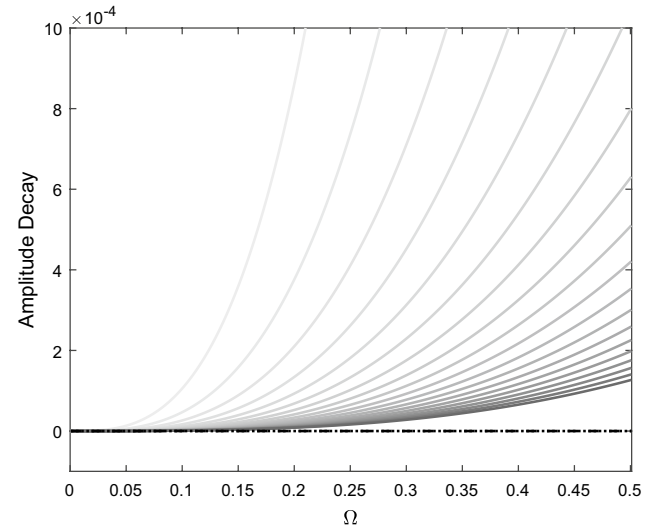
(a)



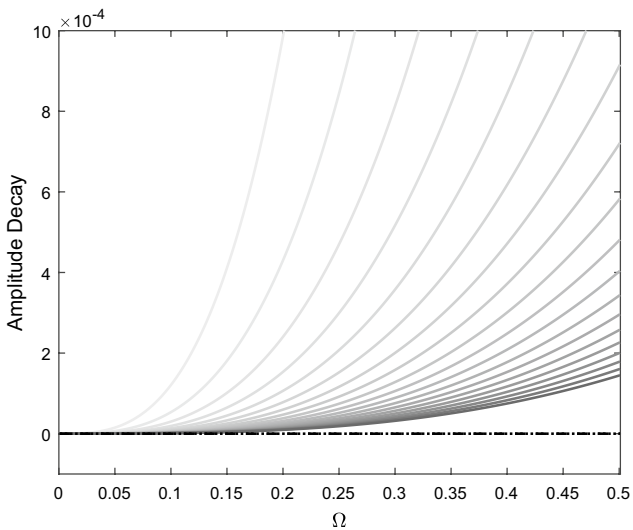
(b)



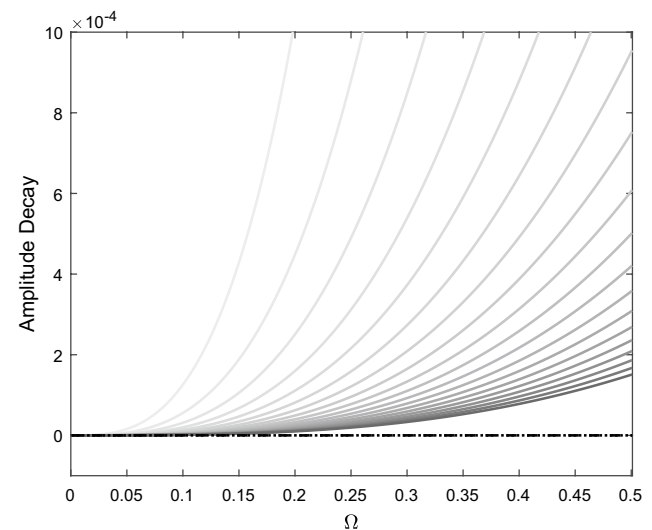
(c)



(d)



(e)



(f)

Fig. 4 Amplitude decay errors for $\Omega_b=1, 1.5, \dots, 10$ (lighter to darker gray color), considering the new methodology with different ρ_b^0 values: **a** 1.0; **b** 0.8; **c** 0.6; **d** 0.4; **e** 0.2; **f** 0.0. Results for the CD and the TR are depicted as black dotted and dashed lines, respectively, for reference. (Color figure online)

spurious non-physical oscillations that sometimes occur due to excitation of spatially unresolved modes. One basic difficulty in designing such dissipative algorithms is to add high-frequency dissipation without introducing excessive algorithmic damping in the important low-frequency modes. By considering these locally-defined adaptive parameters, this difficulty may be better overcome and improved performances obtained.

As discussed, the proposed technique is formulated so that $\Omega_b \equiv \Omega_e^{\max}$ and $\rho_b \equiv \rho_b^0(1 - \xi_e)$. In this case, since $\Omega_b \leq \Omega_c$ (where Ω_c stands for the critical sampling frequency of the method), stability is always provided following the proposed procedure (i.e., Ω_e^{\max} is always less than or equal to Ω_c , ensuring stability). Additionally, for $\mu_1^e = 0$ and $\mu_2^e = 0$ (which is yielded by $\rho_b^0 = 1$ and $\xi_e = 0$, for instance), $\Omega_c = \Omega_b \equiv \Omega_e^{\max}$ and non-dissipative analyses are then performed. In this case, the technique becomes uniquely defined by μ_0^e and, as Eq. (6a) indicates, $\mu_0^e \rightarrow 1/4$ as $\Omega_e^{\max} \rightarrow \infty$. Thus, the technique tends to replicate the TR, as Ω_e^{\max} increases. As Ω_e^{\max} decreases, the period elongation errors provided by the novel approach are reduced, eventually also yielding negative period elongation errors (in fact, the proposed formulation provides an intermediate behaviour between the CD and the TR, for instance, for $0 < \mu_0^e < 1/4$ or, alternatively stated, for $\Omega_e^{\max} > 2$). Thus, taking into account non-dissipative analyses, the new technique (which provides guaranteed stability) is typically more accurate than the TR, which is “the second-order accurate A-stable linear multistep method with the smallest error constant” (Dahlquist’s theorem [36]).

Further details about the new locally-defined time integration procedure, which is determined by Eqs. (5a, 5b, 5c, 5d and 6a, 6b,6c) are provided in the next section, in which the properties of the proposed formulation are discussed. The basic steps of the proposed time-marching solution algorithm are summarized in Table 1, in which Eqs. (5a, 5b, 5c, 5d) are reviewed taking into account a locally-defined approach. As one may observe in this algorithm, the designed solution procedure is very easy to implement and to apply, standing as a quite simple and straightforward formulation, although it is highly flexible and versatile.

3 Properties of the method

In this section, a single degree of freedom (SDOF) problem is considered in order to further discuss the properties (i.e., accuracy, stability etc.) of the proposed technique, following standard guidelines [1]. Of course, since different values are expected to occur along the discretized model for the time integration parameters of the method, a standard modal decomposition correlation is not valid for the proposed formulation. Thus, results are here presented taking into account several different quantities for the input parameter ρ_b^0 , as well as for the sampling frequencies (Ω_e^{\max}) and damping ratios (ξ_e) of the model/method (and, consequently, for μ_0^e, μ_1^e and μ_2^e), aiming to illustrate a basic possible range of behaviours and features that characterizes the discussed locally-defined approach.

The equation of motion for the SDOF model may be written as:

$$\ddot{u}(t) + 2\xi w \dot{u}(t) + w^2 u(t) = f(t) \tag{7}$$

where ξ and w stand for the damping ratio and the natural frequency of the model, respectively. Considering Eq. (7) and the proposed technique, the following recursive relationship can be established for the discussed time-marching solution:

$$\begin{bmatrix} u^{n+1} \\ \dot{u}^{n+1} \end{bmatrix} = \begin{bmatrix} A_{11} & A_{12} \\ A_{21} & A_{22} \end{bmatrix} \begin{bmatrix} u^n \\ \dot{u}^n \end{bmatrix} + \begin{bmatrix} L_1 \\ L_2 \end{bmatrix} \int_{t^n}^{t^{n+1}} f(t) dt = \mathbf{A} \begin{bmatrix} u^n \\ \dot{u}^n \end{bmatrix} + \mathbf{L} \int_{t^n}^{t^{n+1}} f(t) dt \tag{8}$$

where \mathbf{A} and \mathbf{L} stand for the amplification matrix and the load operator vector of the method, respectively, which may be defined as:

$$A_{11} = [1 + \xi w \Delta t - \left(\frac{1}{2} - \mu_0\right) w^2 \Delta t^2 - \frac{1}{2} \mu_1 w^4 \Delta t^4] A \tag{9a}$$

$$A_{12} = [1 - \left(\frac{1}{4} - \mu_0\right) w^2 \Delta t^2 - \frac{1}{2} \mu_2 w^4 \Delta t^4] \Delta t A \tag{9b}$$

$$A_{21} = -(1 + \mu_1 w^2 \Delta t^2) w^2 \Delta t A \tag{9c}$$

$$A_{22} = [1 - \xi w \Delta t - \left(\frac{1}{2} - \mu_0\right) w^2 \Delta t^2 - \mu_2 w^4 \Delta t^4] A \tag{9d}$$

$$L_1 = \frac{1}{2} \Delta t A \tag{10a}$$

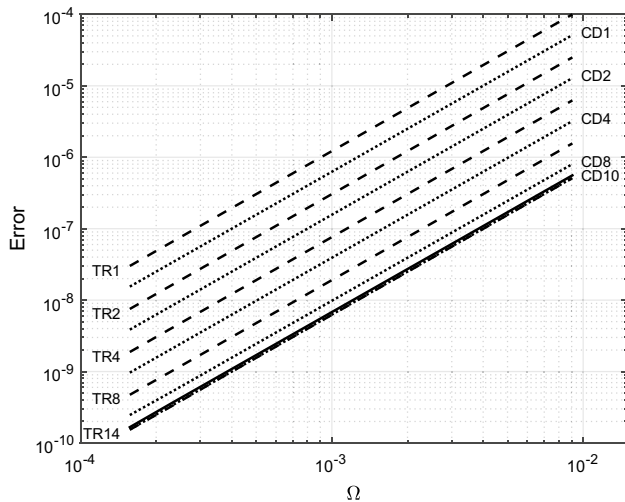


Fig. 5 Convergence analysis considering the n -substep CD (dotted lines, results for $n=1, 2, 4, 8$ and 10 are depicted), the n -substep TR (dashed lines, results for $n=1, 2, 4, 8$ and 14 are depicted), and the new single-step methodology for $\Omega_b=2.46$ and $\rho_b^0=1$ (solid line)

$$L_2 = A \tag{10b}$$

where $A = (1 + \xi w \Delta t + \mu_0 w^2 \Delta t^2)^{-1}$.

Expressions (9a, 9b, 9c, 9d), when expanded in Taylor’s series, provide:

$$A_{11} = 1 - \frac{1}{2} w^2 \Delta t^2 + \frac{1}{2} \xi w^3 \Delta t^3 + \frac{1}{2} (\mu_0 - \mu_1 - \xi^2) w^4 \Delta t^4 + O(\Delta t^5) \tag{11a}$$

$$A_{12} = \Delta t - \xi w \Delta t^2 - \left(\frac{1}{4} - \xi^2\right) w^2 \Delta t^3 + \left(\frac{1}{4} + \mu_0 - \xi^2\right) \xi w^3 \Delta t^4 + O(\Delta t^5) \tag{11b}$$

$$A_{21} = -w^2 \Delta t + \xi w^3 \Delta t^2 + (\mu_0 - \mu_1 - \xi^2) w^4 \Delta t^3 - (2\mu_0 - \mu_1 - \xi^2) \xi w^5 \Delta t^4 + O(\Delta t^5) \tag{11c}$$

$$A_{22} = 1 - 2\xi w \Delta t - \left(\frac{1}{2} - 2\xi^2\right) w^2 \Delta t^2 + \left(\frac{1}{2} + 2\mu_0 - 2\xi^2\right) \xi w^3 \Delta t^3 + \left[\left(\frac{1}{2}\mu_0 - \mu_2\right) - \left(\frac{1}{2} + 4\mu_0\right)\xi^2 + 2\xi^4\right] w^4 \Delta t^4 + O(\Delta t^5) \tag{11d}$$

and, by comparing these expressions to those of the expansion of the analytical amplification matrix A^a :

$$A_{11}^a = 1 - \frac{1}{2} w^2 \Delta t^2 + \frac{1}{3} \xi w^3 \Delta t^3 + \left(\frac{1}{24} - \frac{1}{6} \xi^2\right) w^4 \Delta t^4 + O(\Delta t^5) \tag{12a}$$

$$A_{12}^a = \Delta t - \xi w \Delta t^2 - \left(\frac{1}{6} - \frac{2}{3} \xi^2\right) w^2 \Delta t^3 + \left(\frac{1}{6} - \frac{1}{3} \xi^2\right) \xi w^3 \Delta t^4 + O(\Delta t^5) \tag{12b}$$

$$A_{21}^a = -w^2 \Delta t + \xi w^3 \Delta t^2 + \left(\frac{1}{6} - \frac{2}{3} \xi^2\right) w^4 \Delta t^3 - \left(\frac{1}{6} - \frac{1}{3} \xi^2\right) \xi w^5 \Delta t^4 + O(\Delta t^5) \tag{12c}$$

$$A_{22}^a = 1 - 2\xi w \Delta t - \left(\frac{1}{2} - 2\xi^2\right) w^2 \Delta t^2 + \left(\frac{2}{3} - \frac{4}{3} \xi^2\right) \xi w^3 \Delta t^3 + \left(\frac{1}{24} - \frac{1}{2} \xi^2 + \frac{2}{3} \xi^4\right) w^4 \Delta t^4 + O(\Delta t^5) \tag{12d}$$

one may observe that the proposed technique is second-order accurate, independently of the adopted values for the time integration parameters of the method.

The stability condition requires that matrix \mathbf{A} does not amplify errors as the time step algorithm advances on time. Therefore, to ensure stability, $\rho \leq 1$ must hold, where ρ is the spectral radius of matrix \mathbf{A} , which represents the maximal absolute magnitude of the eigenvalues of the amplification matrix. In the proposed time-marching procedure, the eigenvalues of \mathbf{A} are given by:

$$\lambda_{1,2} = A_1 \pm (A_1^2 - A_2)^{1/2} \tag{13}$$

where A_1 and A_2 stand for half the trace and the determinant of \mathbf{A} , respectively. These terms may be specified as follows, taking into account the discussed formulation:

$$A_1 = \left[1 - \left(\frac{1}{2} - \mu_0\right) \Omega^2 - \frac{1}{4} (\mu_1 + 2\mu_2) \Omega^4\right] A \tag{14a}$$

$$A_2 = \left[1 - \xi \Omega + \mu_0 \Omega^2 + \frac{1}{2} (\mu_1 - 2\mu_2) \Omega^4\right] A \tag{14b}$$

where $\Omega = w \Delta t$ stands for the sampling frequency of the model.

By examining the spectral radius of matrix \mathbf{A} , the time integration parameter μ_0 may be determined as function of the critical sampling frequency of the method (i.e., as function of Ω_c , which is the sampling frequency value under which stability is ensured), considering $\mu_1 = \mu_2 = 0$ and $\xi = 0$. In this case, one has:

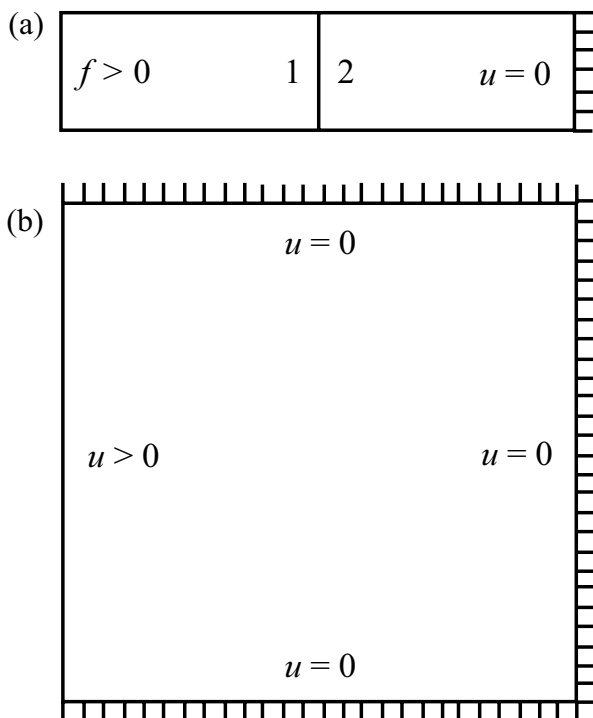


Fig. 6 Sketches of the models: **a** heterogeneous rod (example 1); **b** membrane (example 2)

$$\mu_0 = \frac{1}{4} - \Omega_c^{-2} \tag{15}$$

Analogously, by scrutinizing the spectral radius of matrix **A**, the time integration parameters μ_1 and μ_2 may be specified as function of the bifurcation sampling frequency (i.e., as function of Ω_b , which is the sampling frequency value at which complex conjugate eigenvalues bifurcate into real distinct eigenvalues), in such a way that $\rho_b = \rho_b^0(1 - \xi)$, where ρ_b stands for the bifurcation spectral radius. In this case, one has:

$$\mu_1 = \{(\mu_0 + \xi\Omega_b^{-1} + \Omega_b^{-2})[\rho_b^0(1 - \xi) + 1]^2 - 1\}\Omega_b^{-2} \tag{16a}$$

$$\mu_2 = -\frac{1}{2}\{(\mu_0 + \xi\Omega_b^{-1} + \Omega_b^{-2})[\rho_b^0(1 - \xi) - 1]^2 + [1 - 4(\mu_0 + \Omega_b^{-2})]\}\Omega_b^{-2} \tag{16b}$$

As one may observe, Eqs. (15, 16a, 16b) are used to define μ_0^e , μ_1^e and μ_2^e as indicated in Eqs. (6a, 6b, 6c). In this context, as previously referred, μ_0 , μ_1 and μ_2 may be evaluated for

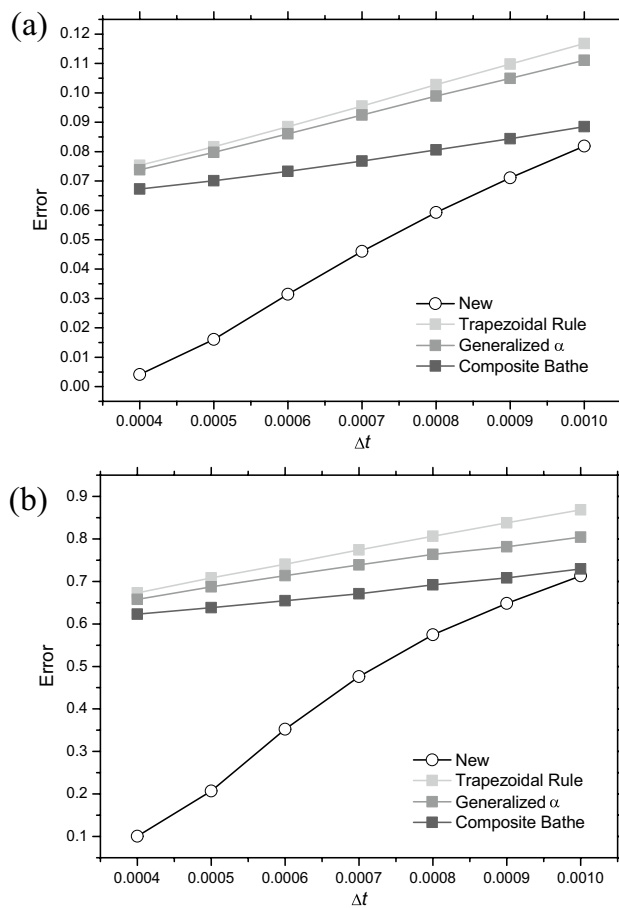


Fig. 7 Error results for the axial **a** displacements and **b** velocities at the middle of the homogeneous rod considering different time-marching procedures and time-step values

each element of the discretized model, imposing the bifurcation sampling frequency of the method (which is simplified to its critical sampling frequency, in a non-dissipative analysis) to equal the maximal sampling frequency of the element. Thus, in the proposed formulation, $\Omega_b \equiv \Omega_e^{\max}$ and $\rho_b \equiv \rho_b^0(1 - \xi_e)$ (which simplifies to $\Omega_c \equiv \Omega_e^{\max}$ and $\rho_b = 1$

once a non-dissipative analysis is regarded). By following this approach, the proposed technique may become very effective dissipating spurious high-frequency modes, as well as counterbalancing errors provided by co-applied spatial

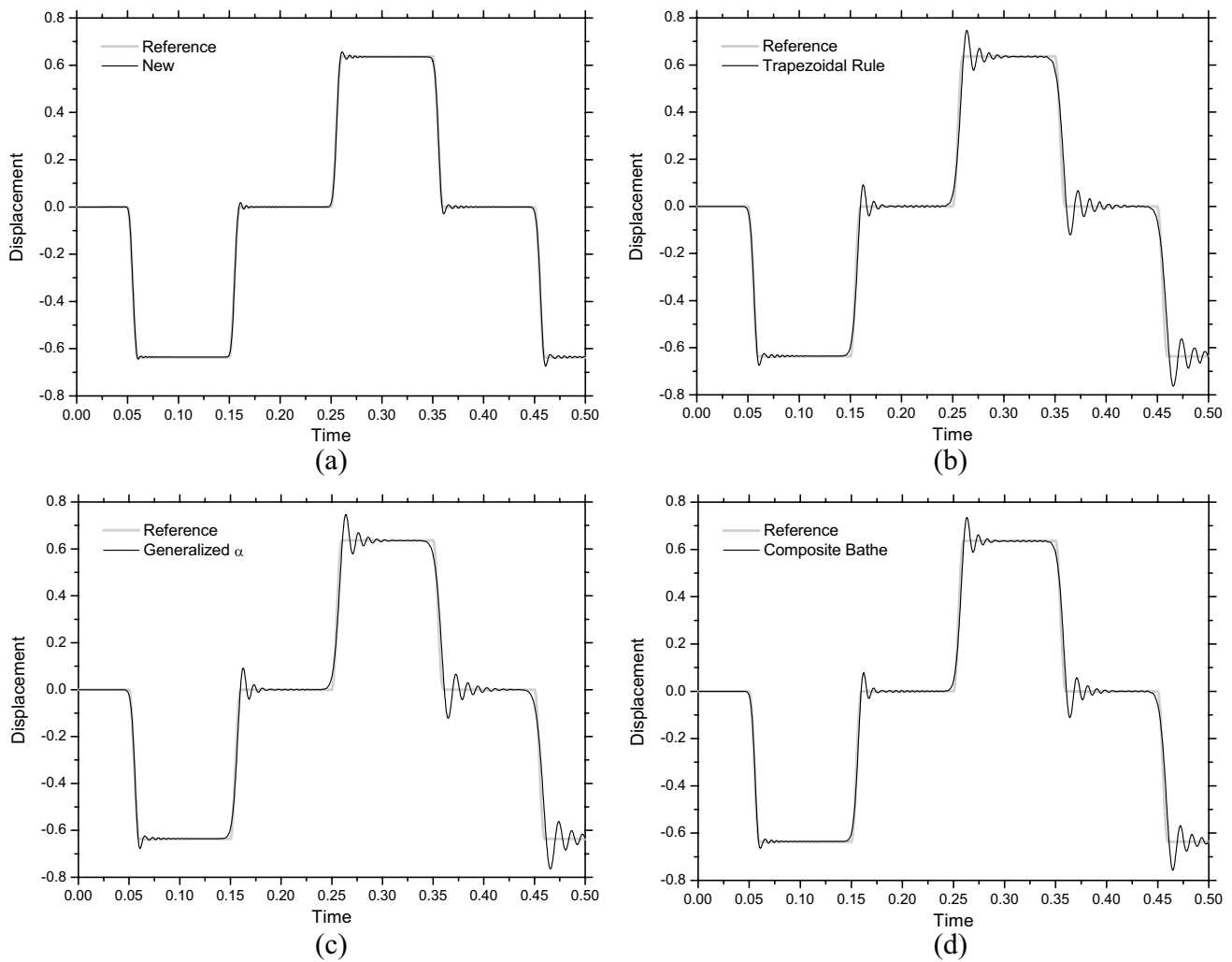


Fig. 8 Time-history results for the axial displacements at the middle of the rod ($\Delta t = 5 \cdot 10^{-4} s$), for $c_2/c_1 = 1$: **a** new; **b** trapezoidal rule; **c** generalized α ; **d** composite Bathe

discretization procedures, rendering a very accurate time-marching formulation.

In Figs. 1 and 2, the spectral radii of the proposed technique are depicted, considering different values for ρ_b^0 , Ω_b and ξ . In these figures, results are provided considering $\rho_b^0 = 0, 0.2, \dots, 1$; $\Omega_b = 1, 1.5, \dots, 10$; and physically undamped ($\xi = 0$) and damped ($\xi = 0.1$) models. Results for the TR and the CD are also depicted in these figures, for reference. As one may observe in Fig. 1a, ρ is never lower than 1 for $\Omega \leq \Omega_c$, once $\rho_b^0 = 1$ and $\xi = 0$ are considered, indicating that numerical and/or physical damping is not introduced into the analysis, in this case. As the selected value for ρ_b^0 decreases, more intense algorithmic damping

is applied, allowing to control the amount of numerical dissipation to be prescribed for the higher frequencies of the model (which, in the proposed technique, are adaptively “tracked” taking into account the different Ω_e^{\max} values of the discretized model), without severely affecting its important low-frequency modes.

In Figs. 3 and 4, standard period elongation and amplitude decay errors [1] are depicted, respectively, considering $\rho_b^0 = 0, 0.2, \dots, 1$ and $\Omega_b = 1, 1.5, \dots, 10$ (as well as $\xi = 0$). In this case, as Fig. 3 illustrates and has been previously highlighted, the period elongation errors of the proposed technique are typically lower than those related to the TR,

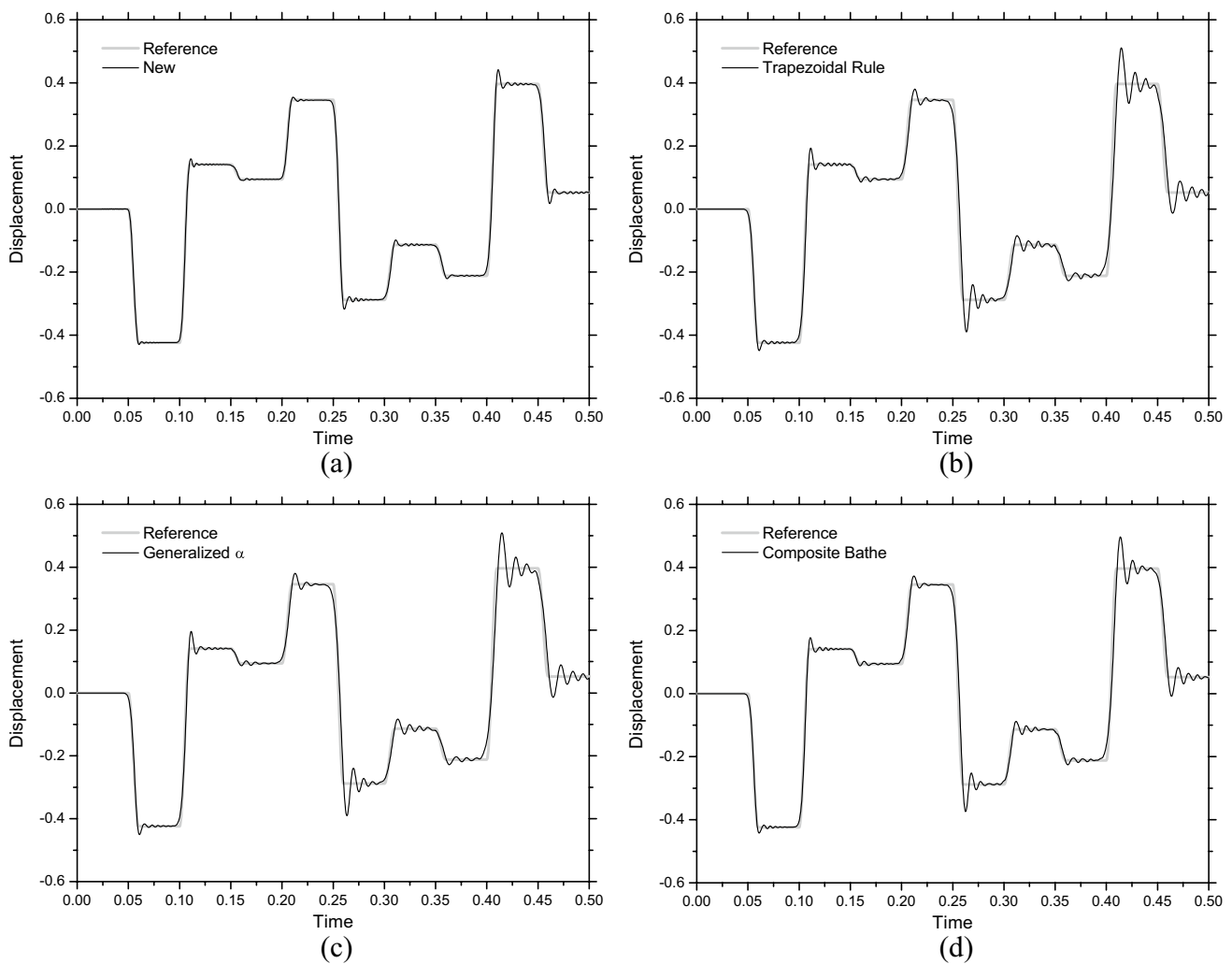


Fig. 9 Time-history results for the axial displacements at the middle of the rod ($\Delta t = 5 \cdot 10^{-4} s$), for $c_2/c_1=2$: **a** new; **b** trapezoidal rule; **c** generalized α ; **d** composite Bathe

describing a very accurate time-marching procedure. As Fig. 3 further indicates, the period elongation errors of the new approach vary from negative to positive values as Ω_b increases and, consequently: (i) extremely small period elongation errors take place for median Ω_b values, providing, in this case, a highly accurate time-marching formulation (this aspect is further illustrated in Fig. 5); (ii) for complex problems, in which several Ω_e^{\max} values occur, the discussed locally-defined time-marching formulation may enable both positive and negative period elongation errors, according to the local features of the model, allowing dispersion errors to be countervailed, further improving the accuracy of the analysis.

Taking into account amplitude decay errors, as Fig. 4 describes, no amplitude decay is induced (as expected) once

$\rho_b^0 = 1$ is adopted (see Fig. 4a). On the other hand, as Fig. 4 also depicts (and is also expected), increasing amplitude decay errors are provided once lower ρ_b^0 values are regarded. Nevertheless, in this case, even when null or low ρ_b^0 values are considered, relative small errors are still provided for the important low-frequency range, highlighting the good performance of the proposed dissipative approach to add high-frequency dissipation without introducing excessive algorithmic damping in the important low-frequency modes.

In Fig. 5, relative error (L2 norm) responses are provided, considering an undamped SDOF model submitted to unit (both displacement and velocity) initial conditions. In this case, results computed by the n -substep TR and CD are also provided in the figure, for reference (in these n -substep solution procedures, n sub-step evaluations are carried out

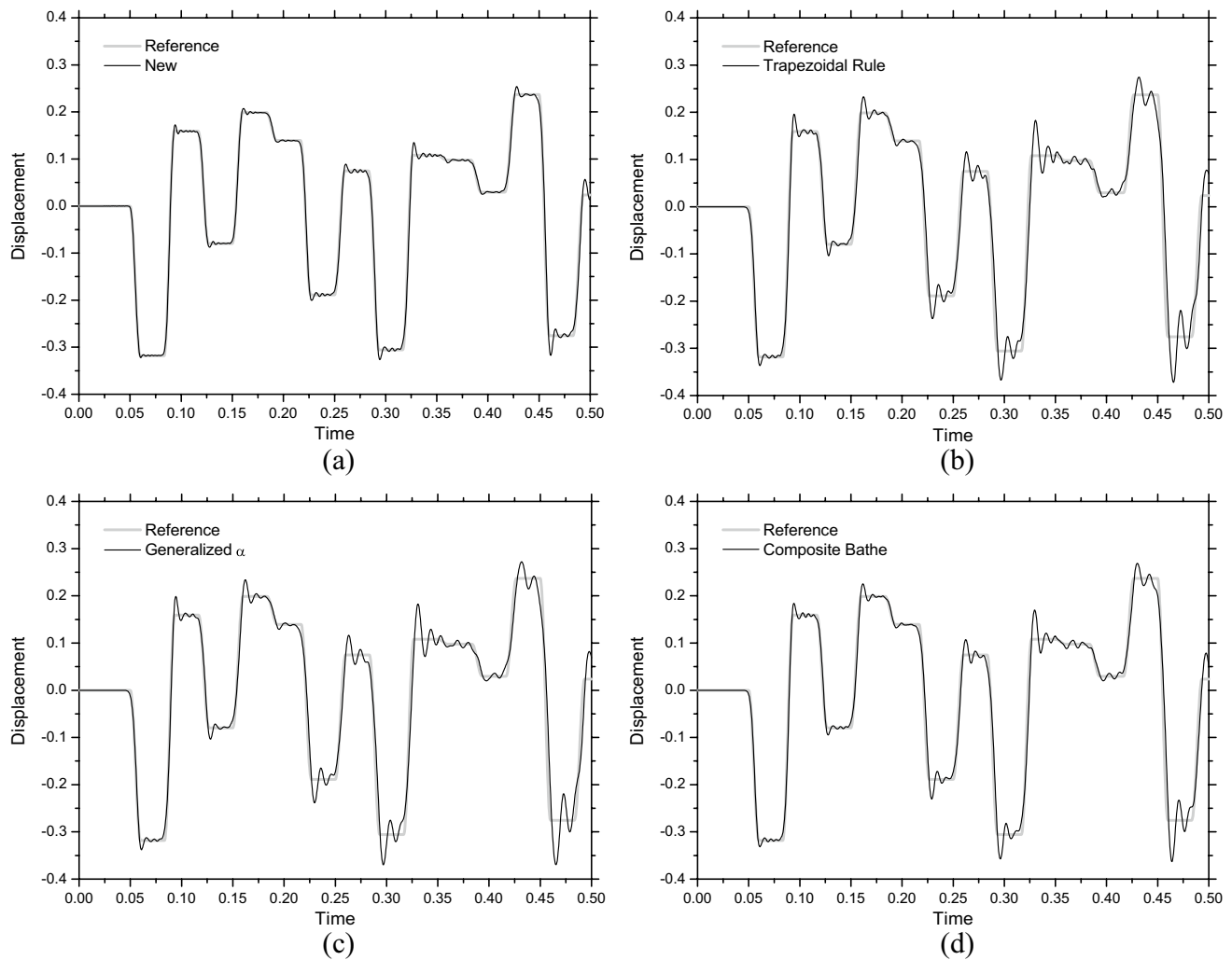


Fig. 10 Time-history results for the axial displacements at the middle of the rod ($\Delta t = 5 \cdot 10^{-4} s$), for $c_2/c_1 = 3$: **a** new; **b** trapezoidal rule; **c** generalized α ; **d** composite Bathe

within a time step of the analysis, by the referred technique, considering a temporal discretization of $\Delta t/n$). As one may observe, the enhanced performance of the novel approach is clearly demonstrated in this figure, which indicates that the proposed single-step formulation may provide significantly more accurate responses than standard multiple-step composite time integration procedures. In fact, as Fig. 5 illustrates, the new technique, considering $\rho_b^0 = 1$ and $\Omega_e^{\max} = 2.46$, is able to compute results that are equivalent to those of the 14-substep TR or to those of the 10-substep CD, highlighting the remarkable effectiveness of the proposed novel approach.

In the next section, numerical results are presented regarding the analyses of various spatially discretized models. For these more complex applications (which are actually

the focus of this paper), the comportment of the proposed time-marching formulation may be better examined, once, for these problems, temporal and spatial discretization procedures act together for solution, allowing several different values for the time integration parameters of the method to concurrently occur along the discretized domain of model.

4 Numerical examples

Two numerical applications are discussed in this section, whose sketches are depicted in Fig. 6. In the first example, the axial motion of a heterogeneous rod is analysed and, in this case, different material and/or numerical properties are applied for different subdomains of the model, allowing to

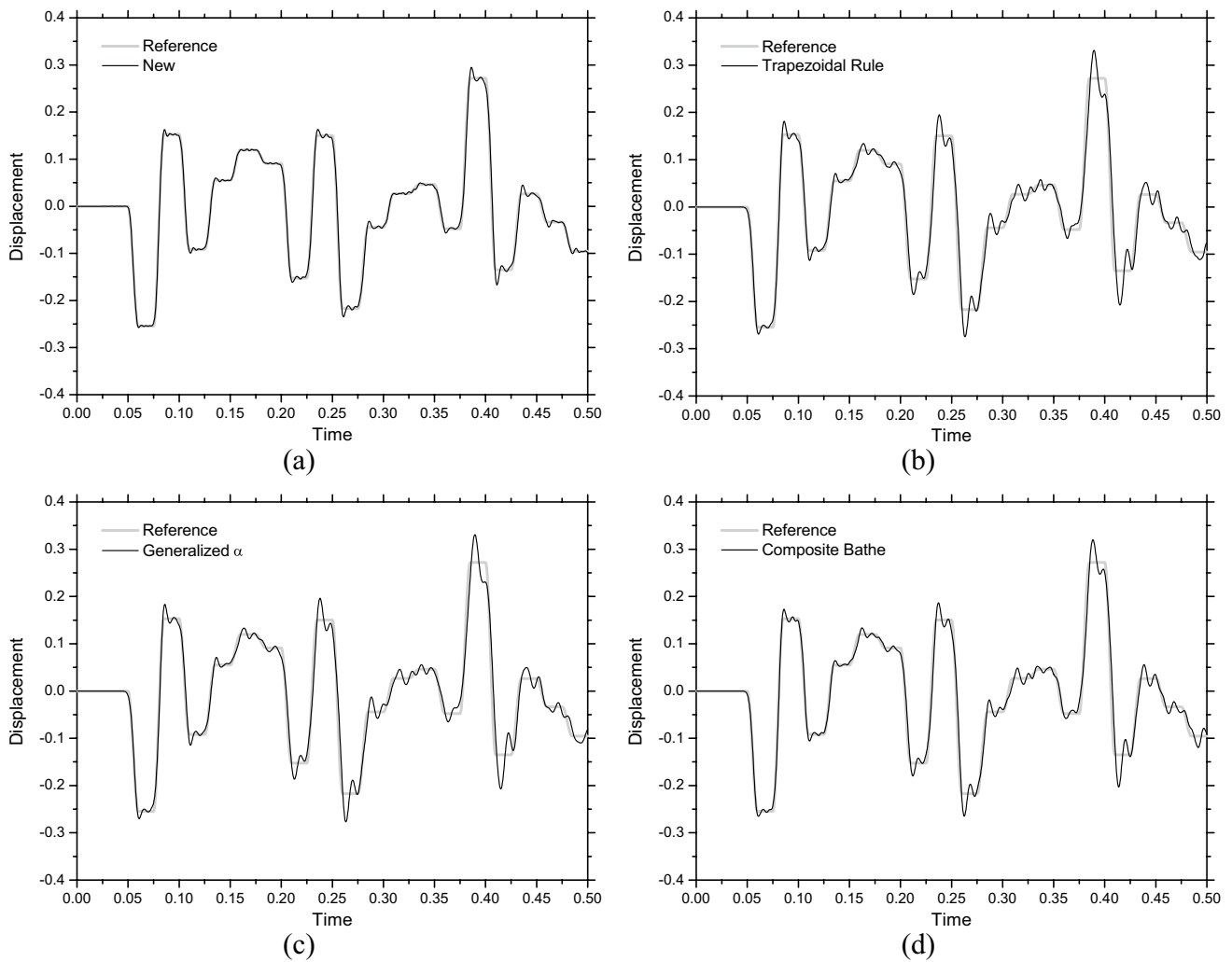


Fig. 11 Time-history results for the axial displacements at the middle of the rod ($\Delta t = 5 \cdot 10^{-4} s$), for $c_2/c_1 = 4$: **a** new; **b** trapezoidal rule; **c** generalized α ; **d** composite Bathe

analyse the performance of the proposed solution procedure for multiple configurations. In the second example, on the other hand, the transversal motion of a homogeneous square membrane is studied and, for this application, an unstructured finite element mesh is adopted for the spatial discretization of the model, allowing several parameters values to co-exist along the discretized domain of the membrane, following a non-trivial distribution. In this case, the versatility and robustness of the proposed locally-defined adaptive procedure may be further analysed, better verifying the effectiveness of the novel formulation.

The responses that are computed by the proposed time-marching technique are compared to those of very well-known time integration procedures, such as the Trapezoidal Rule [13], the Generalized α method [14] (adopting $\rho_\infty = 0.5$), and the Bathe method [15]. The Generalized α

method stands as a dissipative time-integration formulation, whose computational effort is basically the same of the TR, requiring one solver procedure per time step. The Bathe method, on the other hand, stands as a composite dissipative approach, requiring two solver procedures per time step. Thus, its computational effort is basically twice that of the TR or of the Generalized α method. The computed results are also compared to those provided by another locally-defined formulation [28], illustrating the performance of the proposed new approach in comparison to a previously presented equivalent technique.

Analytical answers are available taking into account the two applications that are described in this section [37, 38], allowing to properly evaluate the accuracy of the time-marching formulations that are here considered for solution. Thus, to calculate the relative errors of the computed results,

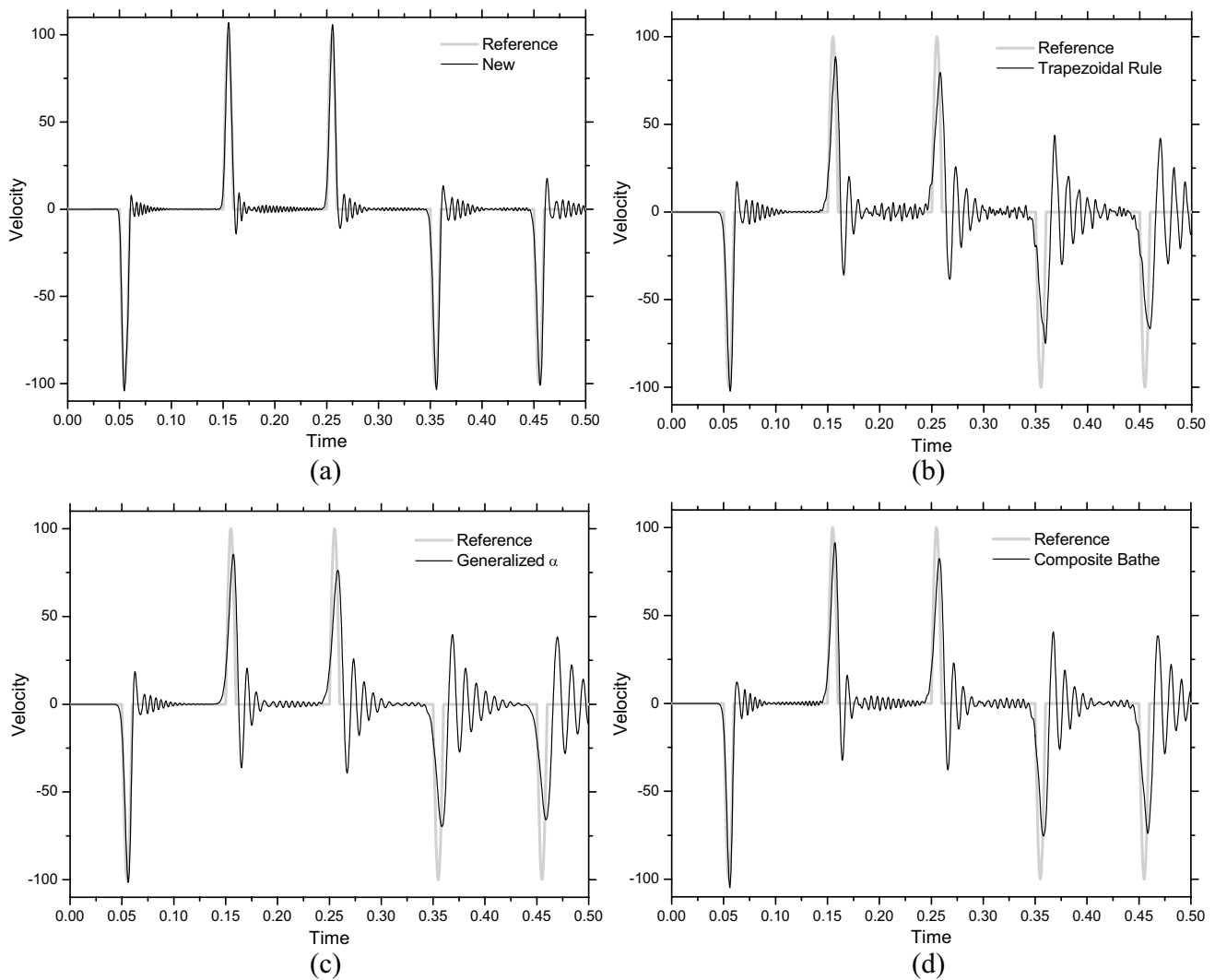


Fig. 12 Time-history results for the axial velocities at the middle of the rod ($\Delta t = 5 \cdot 10^{-4}s$), for $c_2/c_1 = 1$: **a** new; **b** trapezoidal rule; **c** generalized α ; **d** composite Bathe

when comparing the performances of the adopted time integration procedures, the following expression is regarded:

$$Error = \left[\frac{\sum_{n=1}^N (u^n - u_a(t^n))^2}{\sum_{n=1}^N (u_a(t^n))^2} \right]^{1/2} \quad (17)$$

in which u stands for the computed time-history response of a selected degree of freedom, u_a corresponds to its analytical counterpart, and N represents the total number of time steps in the analysis.

As previously observed, the standard Finite Element Method (FEM) [1, 2] is here employed for the spatial discretization of the above-referred models. Notwithstanding, the discussed time integration procedure is not restricted

to be applied associated with this method, and it may be employed in association with any well-established spatial discretization technique that is based on local formulations.

4.1 Example 1

The first application considered in this work is that of a rectangular body behaving like a heterogeneous one-dimensional rod [37]. A sketch of the model is depicted in Fig. 6a. As illustrated in this figure, the rod is fixed at its right border ($x = L$) and subjected to a prescribed axial traction acting on its left border ($x = 0$), which is defined by $f(t) = P \sin(\pi t/T)[H(t) - H(t - T)]$, where $P = 1.0 \text{ kNm}^{-2}$

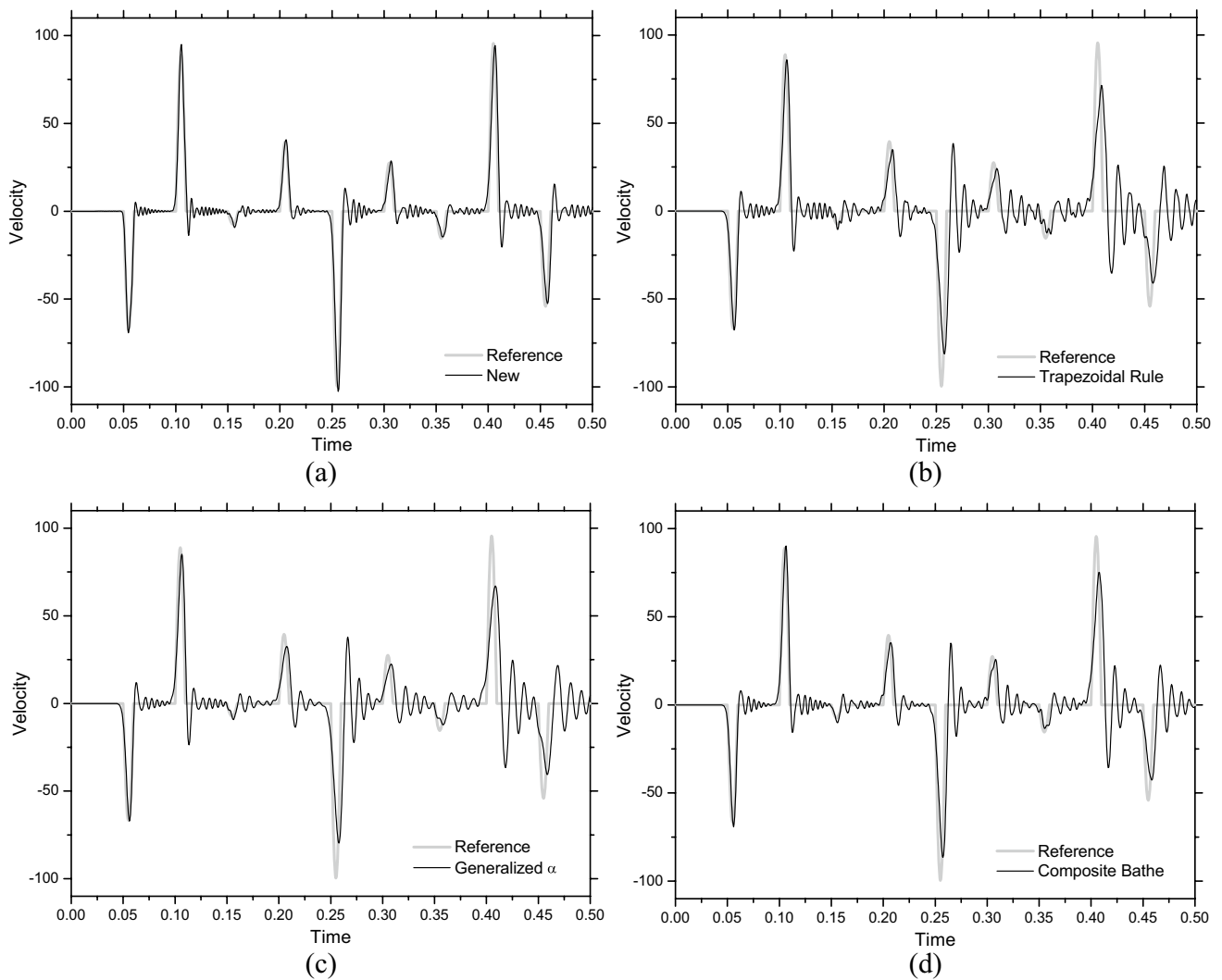


Fig. 13 Time-history results for the axial velocities at the middle of the rod ($\Delta t = 5 \cdot 10^{-4} s$), for $c_2/c_1 = 2$: **a** new; **b** trapezoidal rule; **c** generalized α ; **d** composite Bathe

and $T = 0.01 s$ describe the amplitude and the duration of the applied traction, respectively, and $H(\cdot)$ stands for the Heaviside function. The length of the rod is defined by $L = 1.0 m$, and two equal-sized subdomains compose the referred heterogeneous model, as depicted in Fig. 6a. In this case, whereas the left subdomain of the rod (subdomain 1) is formed by a material whose p-wave propagation velocity is defined by $c_1 = 10 ms^{-1}$, different materials are here employed to characterize the right subdomain of the model (subdomain 2). Thus, in this example, the following values are considered for the p-wave propagation velocity of subdomain 2: (i) $c_2 = 10 ms^{-1}$ (model 1, homogeneous rod); (ii) $c_2 = 20 ms^{-1}$ (model 2); (iii) $c_2 = 30 ms^{-1}$ (model 3); and (iv) $c_2 = 40 ms^{-1}$ (model 4).

A uniform structured FEM mesh with 4000 linear triangular elements is employed to spatially discretize the rod (taking into account a regular 100×20 subdivision of its domain). In this case, for the proposed novel formulation, three layers are considered along the discretized domain of the model, for which different ρ_b^0 values are assigned. Thus, (i) for the first layer, which is delineated by $0 \leq x \leq 10^{-2}L$, $\rho_b^0 = 0$ is applied; (ii) for the second layer, which is defined by $\frac{1}{2}L \leq x \leq (\frac{1}{2} + 10^{-2})L$, $\rho_b^0 = c_1/c_2$ is considered; and, finally, (iii) for the third layer, which is described by the remain of the model, $\rho_b^0 = 1$ is assigned. In this context, numerical damping is applied just on 2% of the domain of the heterogeneous rod (i.e., on a narrow strip of elements next to its loaded border and on an analogous strip next to

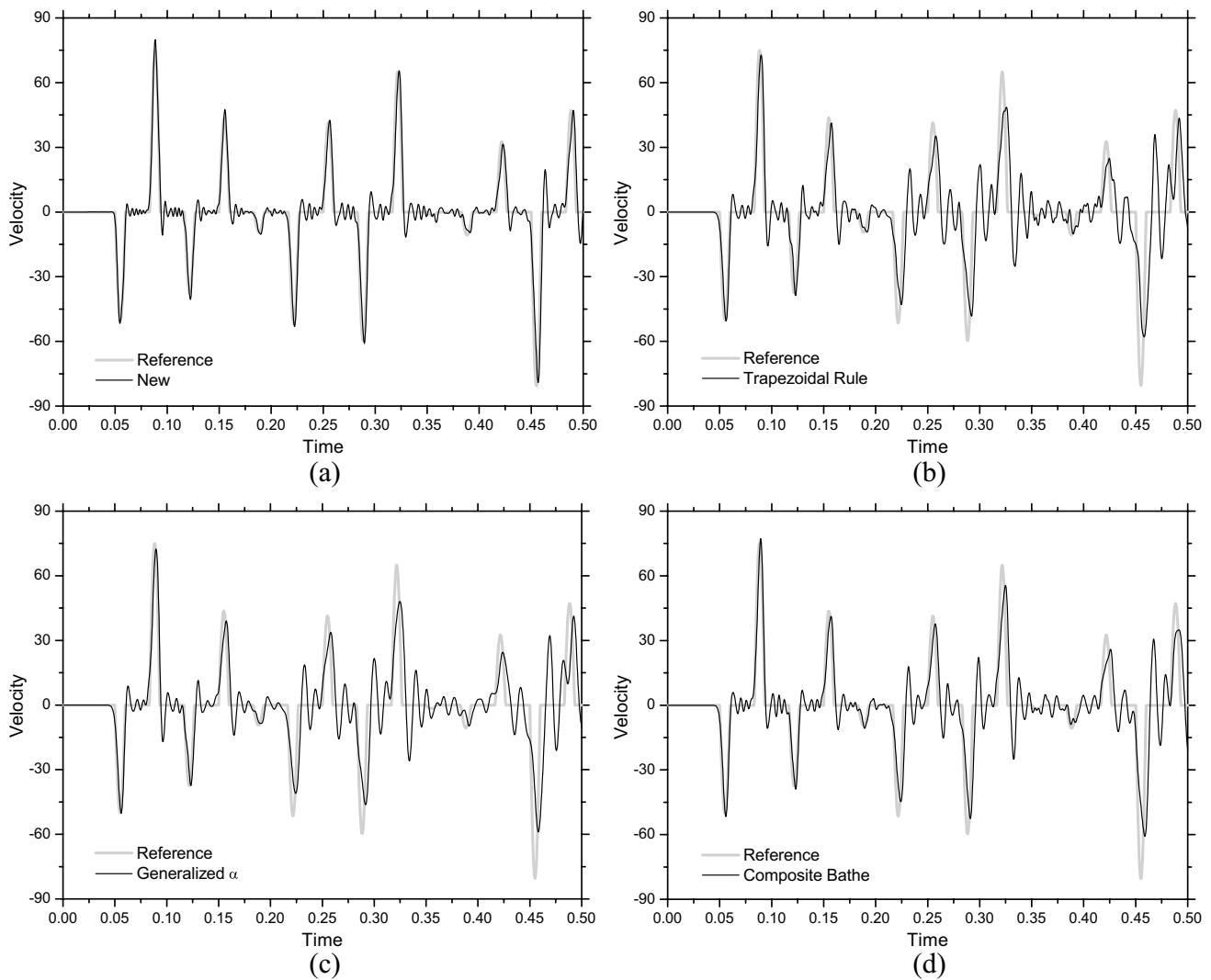


Fig. 14 Time-history results for the axial velocities at the middle of the rod ($\Delta t = 5 \cdot 10^{-4}s$), for $c_2/c_1=3$: **a** new; **b** trapezoidal rule; **c** generalized α ; **d** composite Bathe

its material interface), and on 1% of the domain of the homogeneous rod (i.e., just on a narrow strip of elements next to its loaded border).

Initially, the referred homogeneous rod is studied, and several different time-step values are considered for its analysis. For each one of these adopted Δt values, the relative error of the computed axial displacements and velocities at the middle of the rod ($x = L/2$) is evaluated, following Eq. (17), and depicted in Fig. 7, taking into account the discussed novel approach and the previously referred standard time-marching procedures (similar error results are obtained if other points of the model are considered). As one may observe in this figure, the proposed novel formulation provides exceptionally more accurate responses than the referred standard techniques, even yielding much better

results than the selected composite methodology, which considers two solving procedures per time step.

It is important to observe that the error results that are depicted in the Fig. 7 are related to both the spatial and the temporal discretization methods that are applied in the analysis. Thus, the convergence orders of the selected time integration procedures are not supposed to be reproduced in this figure (as they are, for instance, in Fig. 5), as it describes the behaviour of the adopted conjoint spatial/temporal solution methodology rather than of the adopted time integration procedure.

In Fig. 8, time history results for the axial displacement at the middle of the homogeneous rod (model 1) are depicted, taking into account the referred time integration procedures

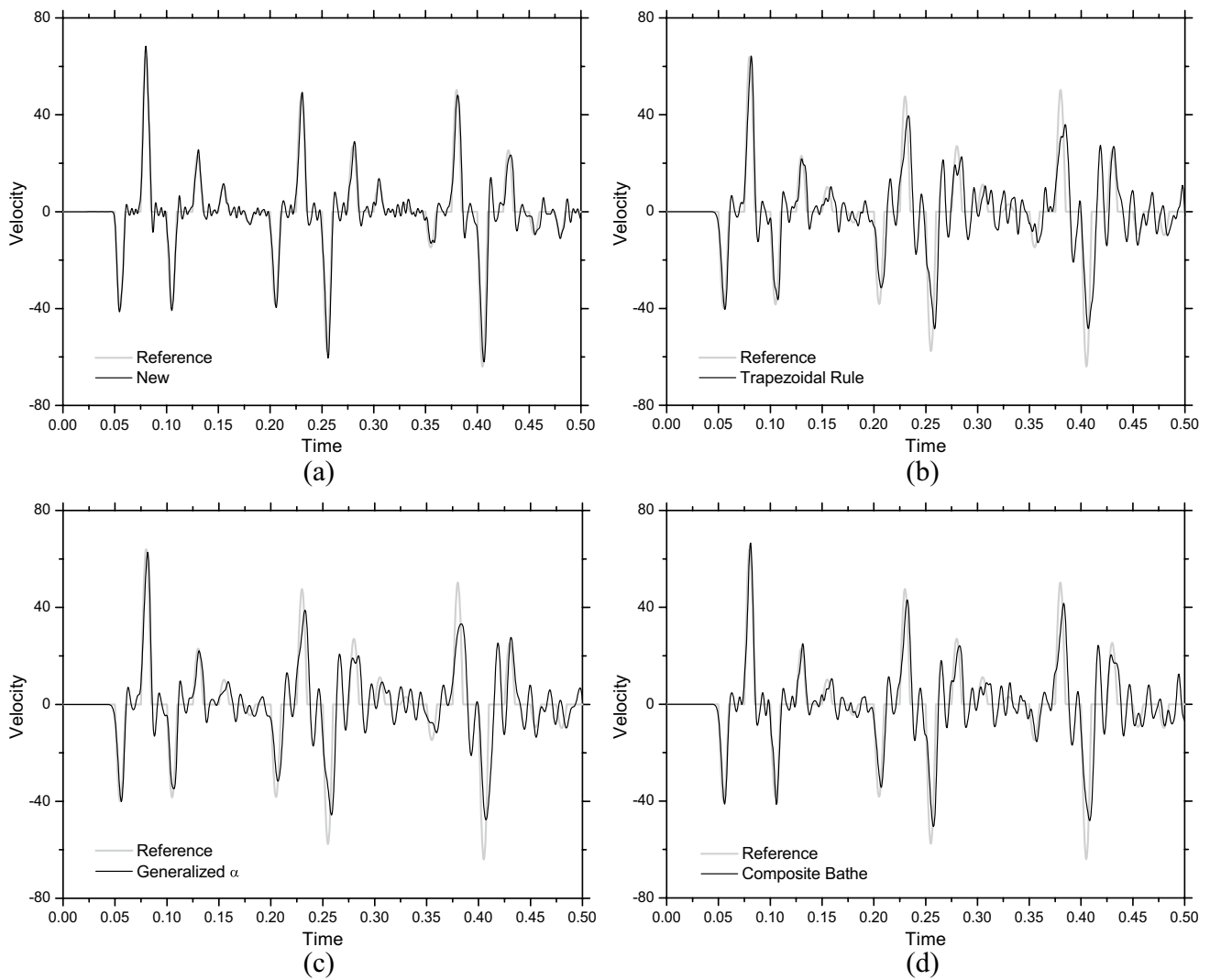


Fig. 15 Time-history results for the axial velocities at the middle of the rod ($\Delta t = 5 \cdot 10^{-4}s$), for $c_2/c_1=4$: **a** new; **b** trapezoidal rule; **c** generalized α ; **d** composite Bathe

Table 2 Computed relative errors for the displacements at the middle of the rod ($\Delta t = 5 \cdot 10^{-4}s$)

Method	c_2/c_1			
	1	2	3	4
New	$1.60 \cdot 10^{-2}$	$3.60 \cdot 10^{-2}$	$5.24 \cdot 10^{-2}$	$5.75 \cdot 10^{-2}$
Trapezoidal rule	$8.16 \cdot 10^{-2}$	$1.12 \cdot 10^{-1}$	$1.57 \cdot 10^{-1}$	$1.75 \cdot 10^{-1}$
Generalized α	$7.98 \cdot 10^{-2}$	$1.09 \cdot 10^{-1}$	$1.55 \cdot 10^{-1}$	$1.72 \cdot 10^{-1}$
Composite bathe	$7.01 \cdot 10^{-2}$	$8.98 \cdot 10^{-2}$	$1.27 \cdot 10^{-1}$	$1.43 \cdot 10^{-1}$

Table 3 Computed relative errors for the velocities at the middle of the rod ($\Delta t = 5 \cdot 10^{-4}s$)

Method	c_2/c_1			
	1	2	3	4
New	$2.07 \cdot 10^{-1}$	$2.75 \cdot 10^{-1}$	$2.84 \cdot 10^{-1}$	$2.69 \cdot 10^{-1}$
Trapezoidal Rule	$7.08 \cdot 10^{-1}$	$6.52 \cdot 10^{-1}$	$6.56 \cdot 10^{-1}$	$6.12 \cdot 10^{-1}$
Generalized α	$6.87 \cdot 10^{-1}$	$6.34 \cdot 10^{-1}$	$6.43 \cdot 10^{-1}$	$5.93 \cdot 10^{-1}$
Composite Bathe	$6.38 \cdot 10^{-1}$	$5.57 \cdot 10^{-2}$	$5.58 \cdot 10^{-1}$	$5.42 \cdot 10^{-1}$

Table 4 Computed relative errors at the middle of the rod considering locally-defined techniques

Type	Method	c_2/c_1			
		1	2	3	4
Displacement	New	$1.60 \cdot 10^{-2}$	$3.60 \cdot 10^{-2}$	$5.24 \cdot 10^{-2}$	$5.75 \cdot 10^{-2}$
	Ref. [28]	$6.20 \cdot 10^{-2}$	$7.88 \cdot 10^{-2}$	$1.15 \cdot 10^{-1}$	$1.32 \cdot 10^{-1}$
Velocity	New	$2.07 \cdot 10^{-1}$	$2.75 \cdot 10^{-1}$	$2.84 \cdot 10^{-1}$	$2.69 \cdot 10^{-1}$
	Ref. [28]	$5.84 \cdot 10^{-1}$	$4.98 \cdot 10^{-1}$	$5.17 \cdot 10^{-1}$	$5.09 \cdot 10^{-1}$

and $\Delta t = 5 \cdot 10^{-4} s$. Analogous results are depicted in Figs. 9, 10, and 11, considering the described heterogeneous model 2, 3, and 4, respectively. Similarly, time history results for the axial velocities at the middle of the rod, for models 1, 2, 3 and 4, are depicted in Figs. 12, 13, 14 and 15, respectively. As these figures illustrate, the proposed locally-defined adaptive technique properly deals with the several configurations that are here considered for the rod, always providing considerably better responses than standard methodologies. The relative error results of the time history responses depicted in Figs. 8, 9, 10 and 11 and in Figs. 12, 13, 14

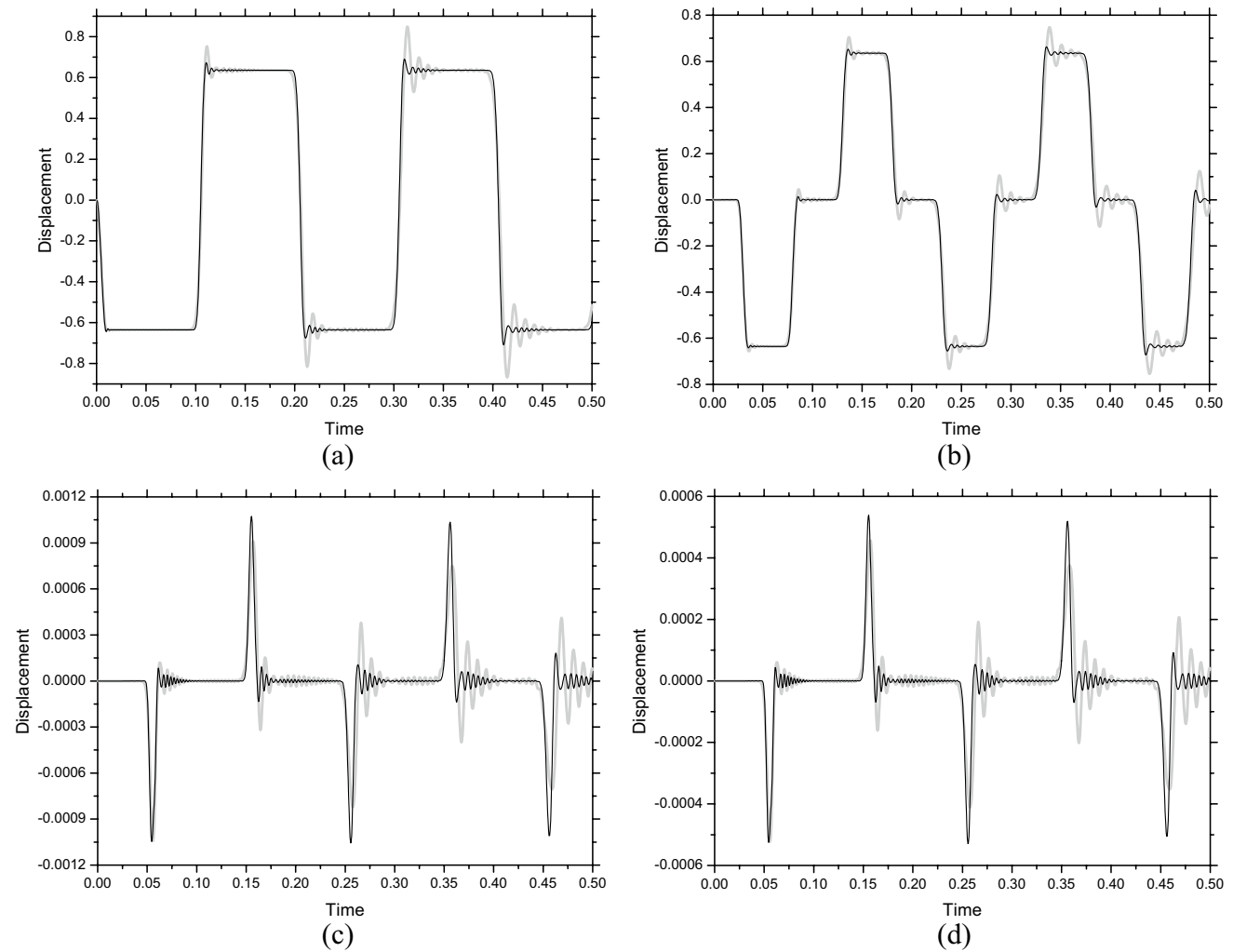


Fig. 16 Time-history results computed by the proposed new methodology (black line) and the composite Bathe method (grey line), for $c_2/c_1 = 100$, at **a** $x=0$ (left border of the rod); **b** $x=L/4$; **c** $x=L/2$; and **d** $x=3L/4$

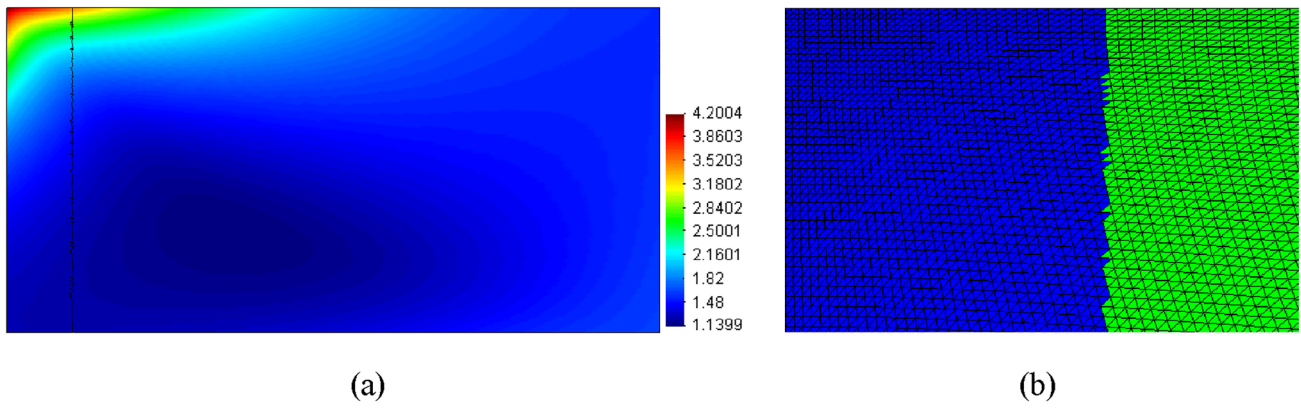


Fig. 17 Sketch of the discretized membrane: **a** Ω_e^{\max} distribution along the model and indication of the selected numerically damped (left) and undamped (right) subdomains; **b** zoomed view of the

upper-left part of the adopted mesh (dissipative elements are depicted in blue and non-dissipative elements are depicted in green). (Color figure online)

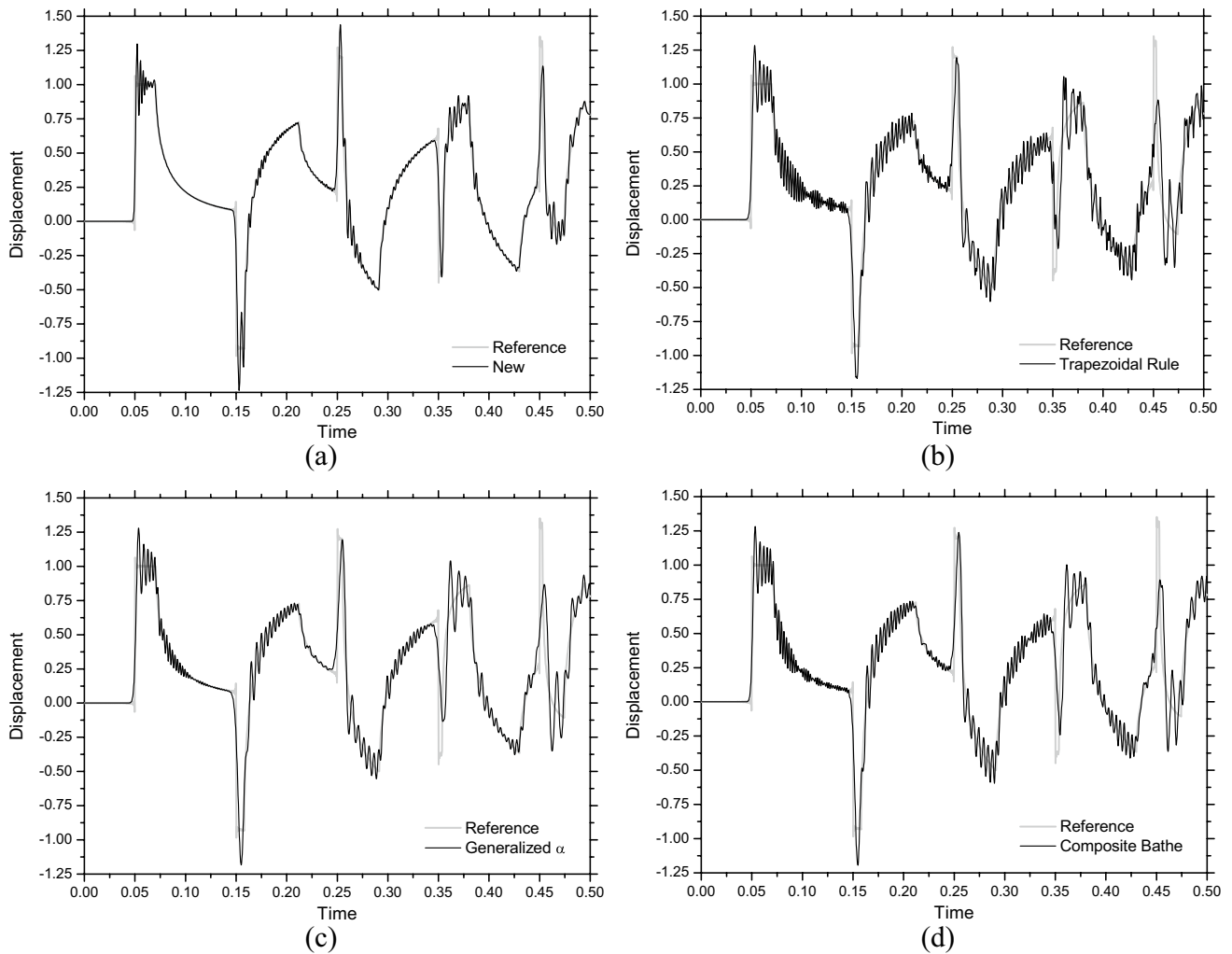


Fig. 18 Time-history results for the transversal displacements at the middle of the membrane: **a** new; **b** trapezoidal rule; **c** generalized α ; **d** composite Bathe

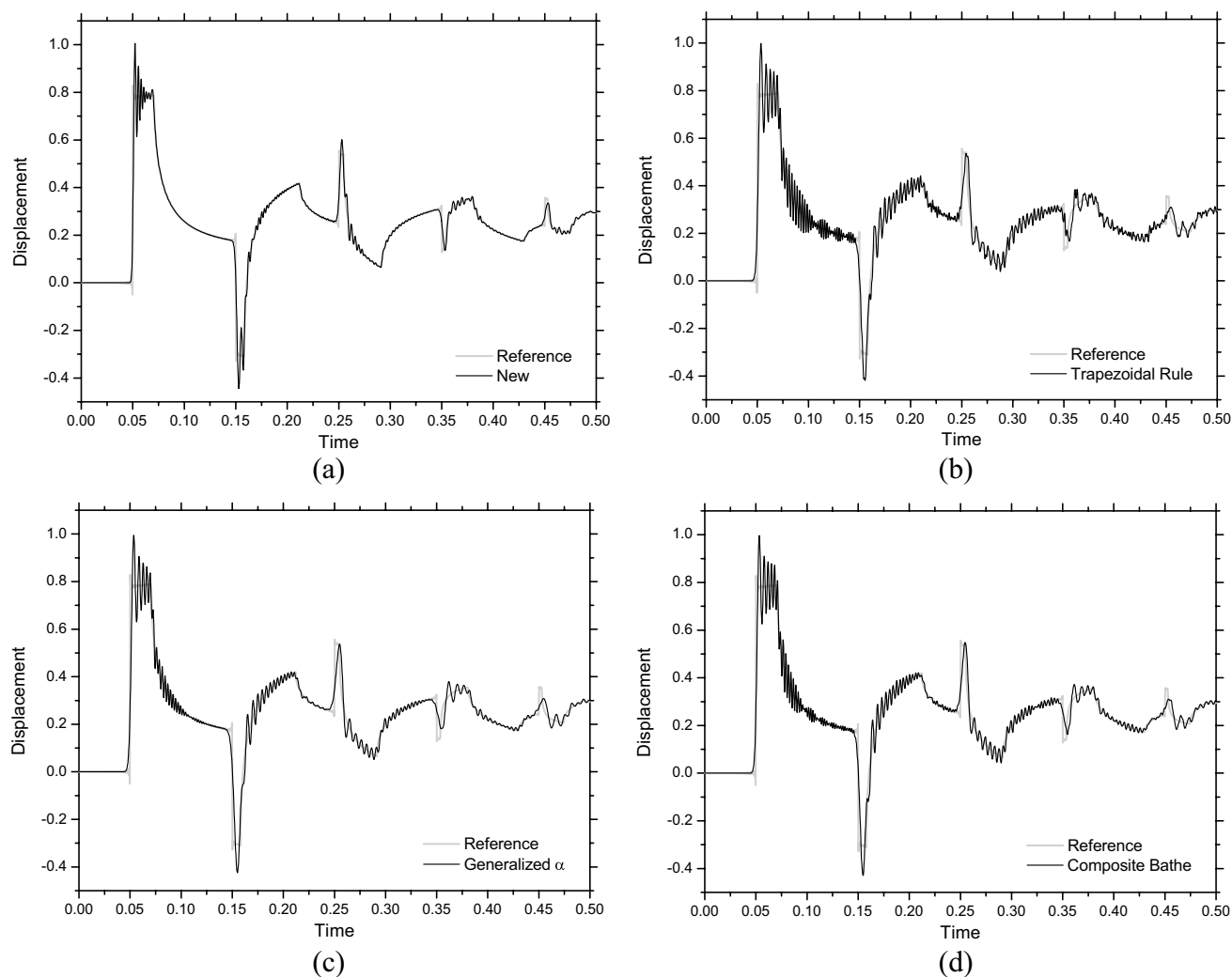


Fig. 19 Time-history results for the transversal displacements at the middle of the membrane (damped model): **a** new; **b** trapezoidal rule; **c** generalized α ; **d** composite Bathe

and 15 are provided in Tables 2 and 3, respectively, further demonstrating the excellent accuracy of the proposed novel approach. As these tables indicate, the errors computed for the novel procedure are approximately 4.4 and 2.5 (Table 2) and 3.1 and 2 (Table 3) times lower than the lowest error computed for the other techniques, considering the referred homogeneous and heterogeneous model, respectively. As one may perceive, these numbers describe a huge difference of performance. In fact, by just comparing the errors computed for these described standard techniques, this relation becomes, at most, less than 1.3. Thus, for the considered analyses, the benefits of the new approach in relation to the composite Bathe method may be considered much greater than the benefits of the composite Bathe method to the TR, for instance. This represents a huge gain of performance for

the novel technique, since its computational effort to analyse the considered rod is basically the same as that of the TR, which is basically half that of the Bathe method. In fact, the computed CPU times for all the above described analyses were basically the same for the novel technique, the TR and the Generalized α method (with a discrepancy of less than 10% between their lowest and highest CPU times, regarding all the performed analyses), which were approximately half that of the composite Bathe method.

In Table 4, the relative error results that are computed considering the locally-defined time-marching technique described in reference [28] are provided, indicating that, as previously highlighted, the presently proposed formulation stands as a more effective solution procedure than equivalent previously presented techniques (although, as described in

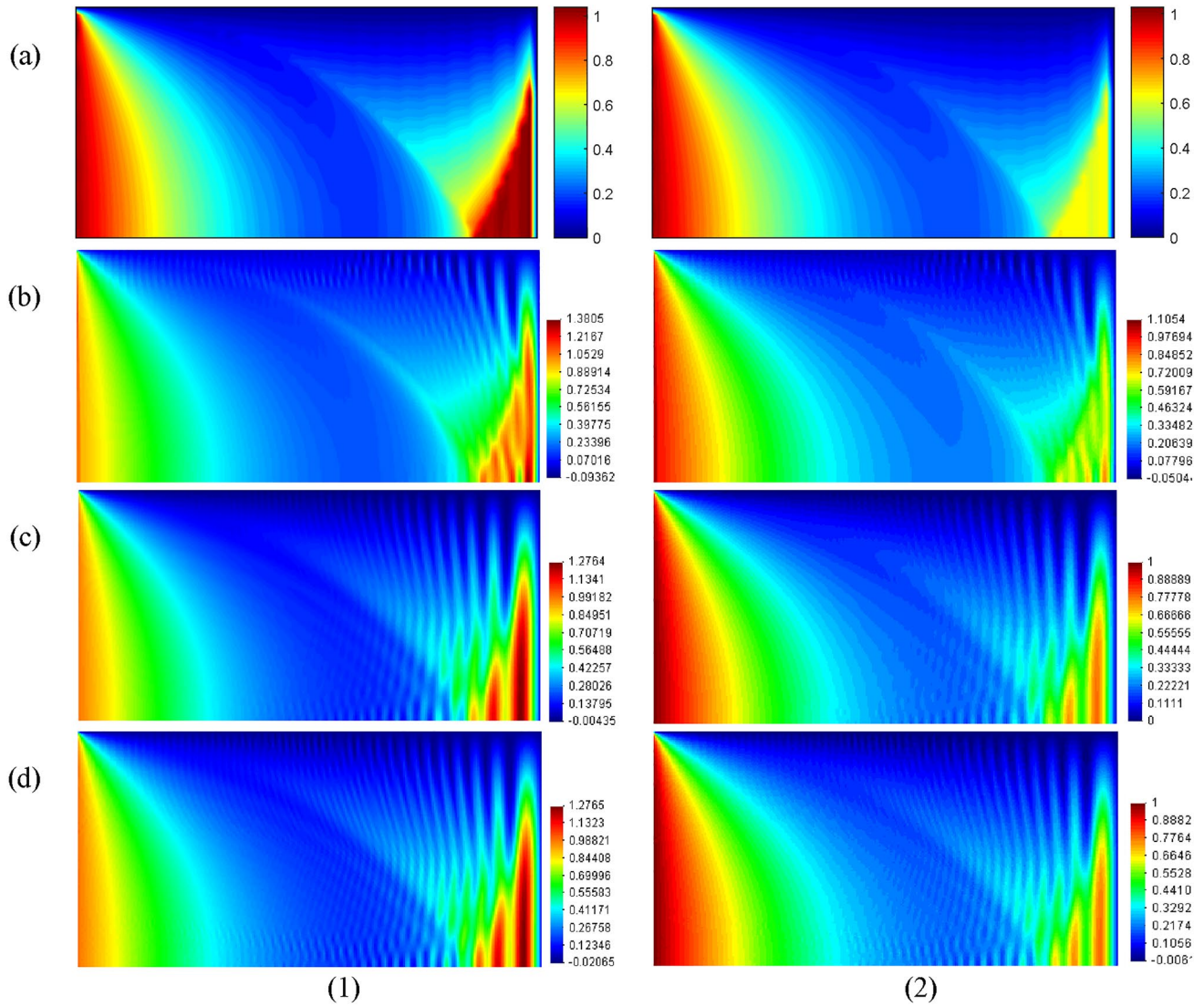


Fig. 20 Computed results along the discretized (1) undamped and (2) damped membrane, at $t=0.1$ s: **a** reference response; **b** new **c** generalized α ; **d** composite Bathe

Table 5 Computed relative errors at the middle of the membrane

Method	Undamped model	Damped model
New	$1.75 \cdot 10^{-1}$	$9.72 \cdot 10^{-2}$
Trapezoidal Rule	$3.06 \cdot 10^{-1}$	$1.54 \cdot 10^{-1}$
Generalized α	$2.83 \cdot 10^{-1}$	$1.40 \cdot 10^{-1}$
Composite Bathe	$2.80 \cdot 10^{-1}$	$1.42 \cdot 10^{-1}$

Table 6 Computed relative errors at the middle of the membrane considering locally-defined techniques

Method	Undamped model	Damped model
New	$1.75 \cdot 10^{-1}$	$9.72 \cdot 10^{-2}$
Ref. [28]	$2.25 \cdot 10^{-1}$	$1.15 \cdot 10^{-1}$

Tables 3 and 4, the formulation described in reference [28] also provides lower errors than standard approaches).

It is interesting to observe that the novel technique may also compute considerably more accurate responses than standard explicit formulations. To illustrate this fact, for $c_2/c_1 = 1$ and $c_2/c_1 = 2$, for instance, stable analyses may be enabled considering the composite explicit technique provided by Noh and Bathe [21], allowing to compute relative errors of $6.02 \cdot 10^{-2}$ and $7.05 \cdot 10^{-2}$ for displacements and of $5.76 \cdot 10^{-1}$ and $4.66 \cdot 10^{-1}$ for velocities, respectively, which are, once again, considerably larger than those of the new technique.

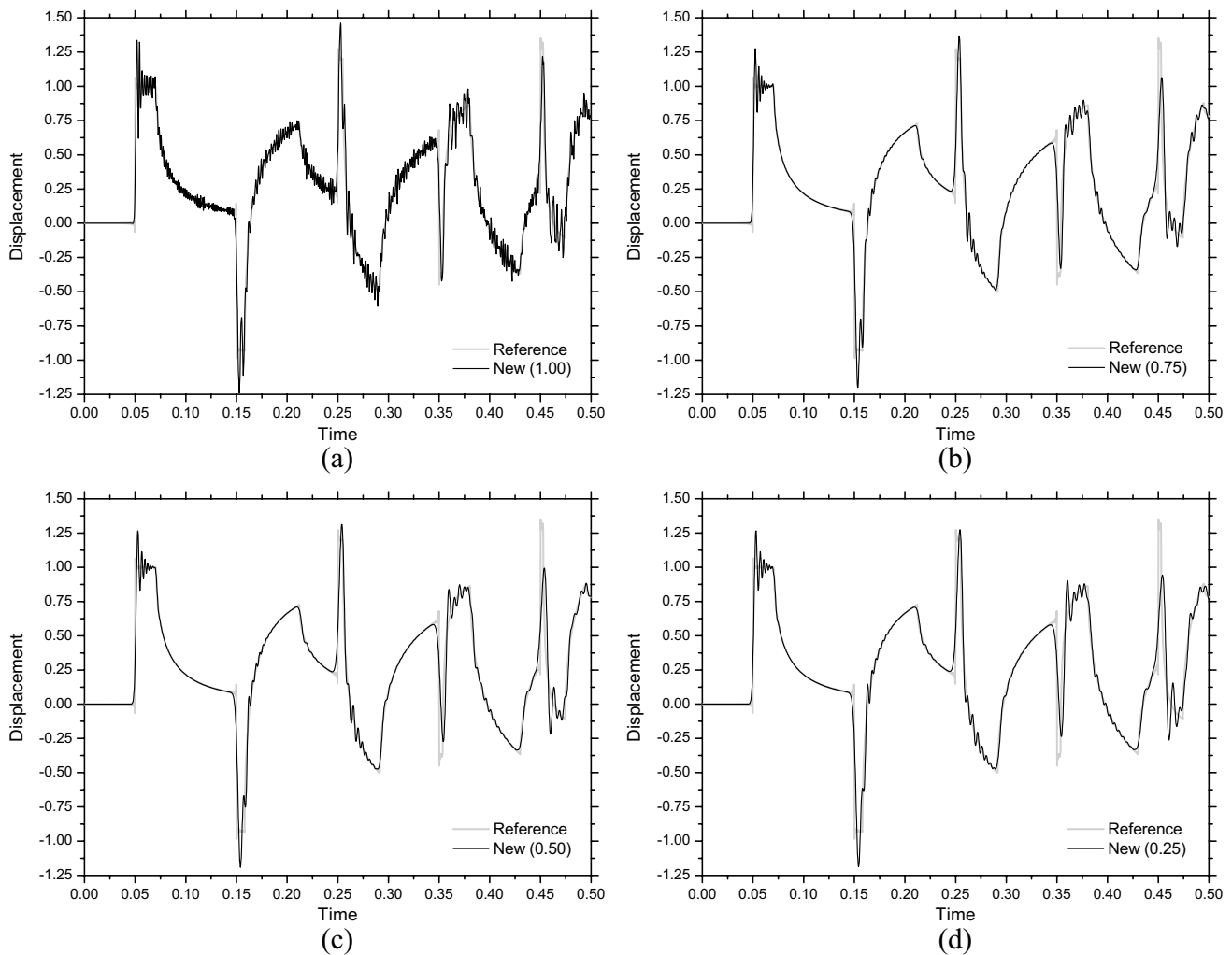


Fig. 21 Time-history results for the transversal displacements at the middle of the membrane considering the new methodology with different ρ_b^0 values (for the entire domain of the model): **a** 1.00; **b** 0.75; **c** 0.50; **d** 0.25

Finally, in Fig. 16, time history results for the axial displacement at four different points of the rod are depicted, for the novel approach and for the composite Bathe method, considering a highly heterogeneous model (i.e., $c_1 = 10 \text{ ms}^{-1}$ and $c_2 = 1000 \text{ ms}^{-1}$). For this configuration, as illustrated in this figure, the novel technique still provides much more accurate responses than the referred composite method, rendering results with fewer spurious non-physical oscillations, as well as with fewer amplitude decay errors (describing a combination that, although ideally pursued, is hardly achieved).

4.2 Example 2

In this second application, the transversal motion of a homogeneous square membrane is analysed [38]. The membrane is fixed at its inferior ($y = 0$), superior ($y = L$) and right

($x = L$) borders and, at its left ($x = 0$) boundary, $u(t) = H(t)$ is prescribed. A sketch of the model is depicted in Fig. 6b. The geometry of the membrane and its wave propagation velocity are defined by $L = 1.0 \text{ m}$ and $c = 10 \text{ ms}^{-1}$, respectively. The symmetry of the model is regarded and just its upper half is spatially discretized, considering a FEM mesh composed by 40,000 linear triangular elements. For this application, since a discontinuity of the boundary conditions occurs at the upper left ($x = 0, y = L$) corner of the discretized model, refinement is applied towards this region. For the proposed novel formulation, initially, two layers are considered along the discretized domain of the membrane, for which different ρ_b^0 values are assigned. In this context, (i) for the first layer, which is characterized by $0 \leq x \leq 10^{-1}L$, $\rho_b^0 = 0$ is applied; and, (ii) for the second layer, which is represented by the remain of the model, $\rho_b^0 = 1$ is considered. The adopted time-step value for this

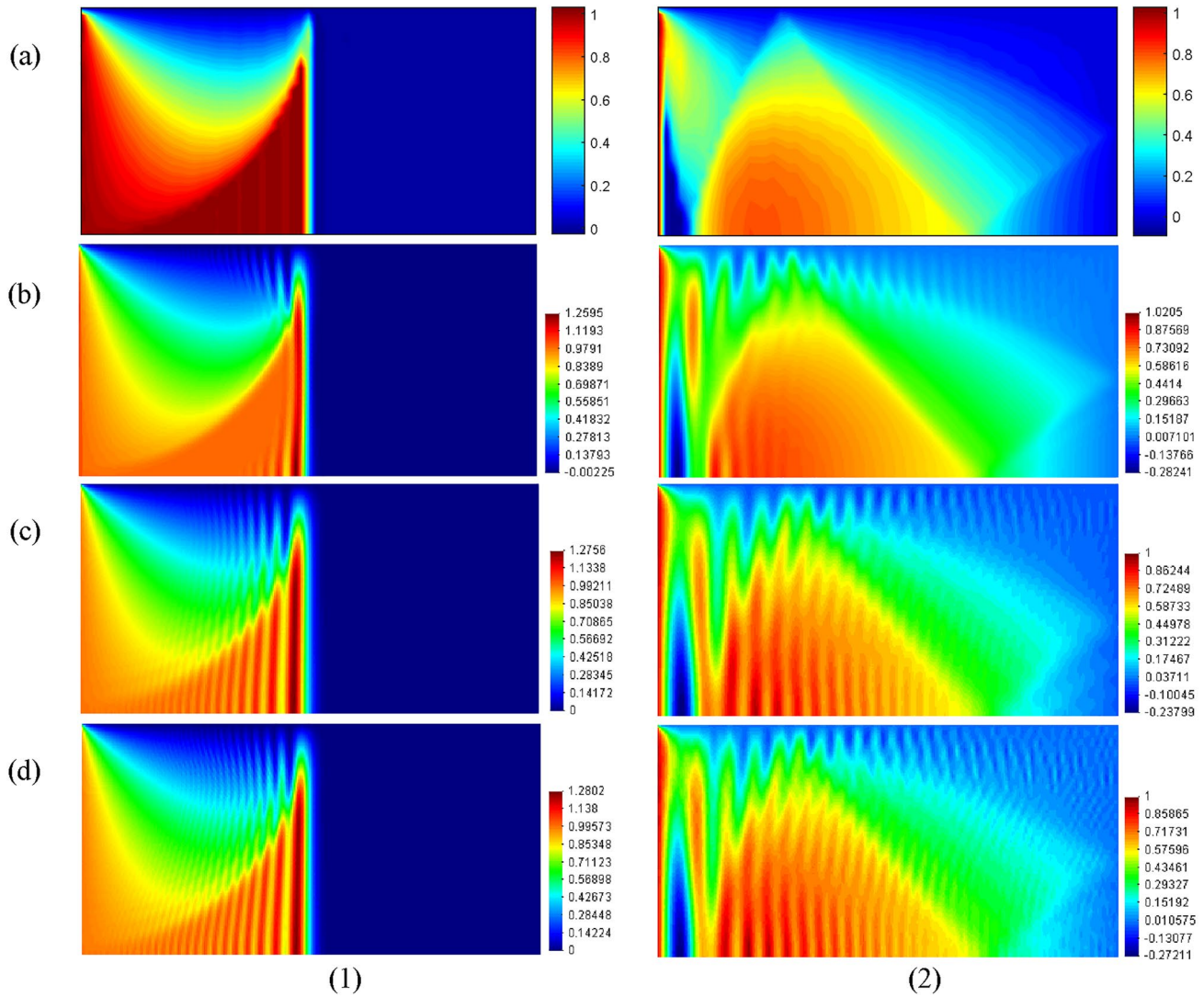


Fig. 22 Computed results along the discretized membrane, at (1) $t = 0.05$ s and (2) $t = 0.20$ s: **a** reference response; **b** new (0.50) **c** generalized α ; **d** composite Bathe

application is $\Delta t = 2.5 \cdot 10^{-4}$ s. The computed Ω_e^{\max} values for these referred spatial and temporal discretizations are depicted in Fig. 17. This figure also illustrates the considered subdomains for ρ_b^0 and provides a partial view of the adopted FEM mesh. As indicated in Fig. 17 (and expected), the values of Ω_e^{\max} vary towards the upper left corner of the membrane, following the refinement of the adopted mesh.

Time-history results for the computed displacements at the middle ($x = y = L/2$) of the membrane are depicted in Fig. 18, taking into account the previously referred time-marching formulations. As this figure illustrates, the proposed novel technique is able to better diminish the non-physical oscillations of the problem, as well as to avoid

excessive algorithmic damping, providing more accurate responses than the referred standard time-marching procedures. Analogous results are depicted in Fig. 19, considering a physically damped model (i.e., $\zeta \neq 0$). In this case, once again the new approach is able to provide better responses, more properly extinguishing spurious oscillations and better avoiding numerical dissipative and dispersive errors. These aspects are further illustrated in Fig. 20, in which computed displacement results along the discretized domain of the model are depicted, for $t = 0.1$ s. The relative error results of the time history responses described in Figs. 18 and 19 are provided in Table 5, further demonstrating the better accuracy of the proposed novel approach. As this table indicates, the errors computed for the novel procedure

are approximately 1.6 (undamped model) and 1.5 (damped model) times lower than the lowest error computed for the standard techniques, indicating once again the great gain in performance provided by the new formulation (in fact, by just comparing the errors computed for the described standard techniques, this relation becomes, at most, 1.1).

As described in Table 4, the relative error results that are computed by the locally-defined time-marching procedure reported in reference [28] are, as well, provided in Table 6 for this second application, indicating once again the better performance of the novel approach in relation to this previously presented technique.

In Fig. 21, time-history results for the computed displacements at the middle of the undamped membrane are depicted, considering a unique value for the input parameter ρ_b^0 of the novel approach, which is assigned for the entire domain of the model. In this case, results for $\rho_b^0 = 1$ (non-dissipative analysis), as well as for $\rho_b^0 = 0.75$, $\rho_b^0 = 0.5$ and $\rho_b^0 = 0.25$ (dissipative analyses), are depicted, allowing to evaluate the performance of the proposed solution technique considering different amounts of applied algorithmic damping. Results for $\rho_b^0 = 0.5$ are further provided in Fig. 22, in which computed displacement responses along the discretized domain of the model, at $t = 0.05$ s and $t = 0.2$ s, are depicted, allowing to compare once more the accuracy of the novel approach to those of standard techniques.

As Figs. 18, 19, 20, 21, 22 illustrate, the proposed locally-defined adaptive formulation properly deals with the spatially unresolved higher modes of the model, suitably diminishing the non-physical oscillations that arise on the computed responses without significantly affecting the contribution of the important lower modes, providing more accurate solutions than standard time-marching techniques.

5 Conclusions

In this paper, a locally-defined time-marching procedure is proposed for dynamic analysis. The discussed technique considers a second-order accurate, truly self-starting, single-step, single-solver, solution algorithm to recursively compute the displacements and velocities of the model. Numerical accelerations are also locally computed in the proposed formulation, taking into account local matrix–vector multiplications just on subdomains where dissipative analyses are to be performed. In fact, as discussed in the proposed procedure, the three time integration parameters of the method are locally determined following the local properties of the discretized model and the input parameter ρ_b^0 , which controls the amount of numerical damping to be introduced into the analysis. Thus, in the reported technique, ρ_b^0 may be provided by the user as an additional “material” parameter (similarly

to those defining the physical properties of the model), locally delineating the numerical features of the considered solution procedure. In this context, a much more versatile time integration methodology is enabled, allowing more flexible analyses to be carried out, and enhanced accuracy provided.

As illustrated in the previous section, the proposed technique is highly accurate, always providing much better results than standard approaches, even considering composite time-marching procedures. In fact, as reported, in the proposed locally-defined adaptive formulation, $\Omega_b \equiv \Omega_e^{\max}$ and $\rho_b \equiv \rho_b^0(1 - \xi_e)$. Thus, for any given time-step value, all elements of the model operate as if in their bifurcation state, ensuring stability for the analyses and establishing a link between the adopted spatial and temporal discretization procedures, allowing their errors to be better counterbalanced and more accurate responses computed. In this context, as it has been illustrated, the technique also provides a very effective self-adjustable dissipative approach, allowing higher frequencies to be “tracked” and, consequently, the influence of the spatially unresolved higher modes of the model to be properly damped (diminishing spurious non-physical oscillations that may arise on the computed responses), without significantly affecting the contribution of the important lower modes, further enhancing the accuracy of the proposed technique.

As described in Table 1, the discussed locally-defined adaptive procedure is also quite simple to implement and to apply, rendering a very straightforward time-marching formulation that avoids complex subdomain definitions and interface treatments between regions in which different numerical features are to be considered. In fact, as discussed in this manuscript, the proposed technique provides several positive attributes that are usually required from an effective time-marching formulation, standing as a very attractive solution methodology for dynamic analysis.

Acknowledgements The financial support by CNPq (Conselho Nacional de Desenvolvimento Científico e Tecnológico) and FAPEMIG (Fundação de Amparo à Pesquisa do Estado de Minas Gerais) is greatly acknowledged.

Data availability It is not applicable.

Declarations

Conflict of interest The author declares that he has no known competing financial interests or personal relationships that could have appeared to influence the work reported in this paper.

References

1. Hughes TJR (2000) The finite element method: linear static and dynamic finite element analysis. Dover Publications INC., New York
2. Bathe KJ (1996) Finite element procedures. Prentice Hall, NJ

3. Zienkiewicz OC, Xie YM (1991) A simple error estimator and adaptive time stepping procedure for dynamic analysis. *Earthquake Eng Struct Dynam* 20:871–887
4. Choi CK, Chung HJ (1996) Error estimates and adaptive time stepping for various direct time integration methods. *Comput Struct* 60:923–944
5. Logg A (2004) Multi-adaptive time-integration. *Appl Numer Math* 48:339–354
6. Rossi DF, Ferreira WG, Mansur WJ, Calenzani AFG (2014) A review of automatic time-stepping strategies on numerical time integration for structural dynamics analysis. *Eng Struct* 80:118–136
7. Wang Y, Zhang T, Zhang X, Mei S, Xie N, Xue X, Tamma K (2022) On an accurate A-posteriori error estimator and adaptive time stepping for the implicit and explicit composite time integration algorithms. *Comput Struct* 266:106789
8. Daniel WJT (1997) Analysis and implementation of a new constant acceleration subcycling algorithm. *Int J Numer Meth Eng* 40:2841–2855
9. Gravouil A, Combescure A (2001) Multi-time-step explicit-implicit method for non-linear structural dynamics. *Int J Numer Meth Eng* 50:199–225
10. Soares D, Mansur WJ, Lima DL (2007) An explicit multi-level time-step algorithm to model the propagation of interacting acoustic-elastic waves using finite element/finite difference coupled procedures. *Comput Model Eng Sci* 17:19–34
11. Dujardin G, Lafitte P (2016) Asymptotic behaviour of splitting schemes involving time-subcycling techniques. *IMA J Numer Anal* 36:1804–1841
12. Pinto LR, Soares D, Mansur WJ (2021) Elastodynamic wave propagation modelling in geological structures considering fully-adaptive explicit time-marching procedures. *Soil Dyn Earthq Eng* 150:106962
13. Newmark NM (1959) A method of computation for structural dynamics. *J Eng Mech Division ASCE* 85:67–94
14. Chung J, Hulbert JM (1993) A time integration method for structural dynamics with improved numerical dissipation: the generalized α method. *J Appl Mech* 30:371–375
15. Bathe KJ, Baig MMI (2005) On a composite implicit time integration procedure for nonlinear dynamics. *Comput Struct* 83:2513–2534
16. Soares D (2017) A simple and effective single-step time marching technique based on adaptive time integrators. *Int J Numer Meth Eng* 109:1344–1368
17. Liu T, Huang F, Wen W, He X, Duan S, Fang D (2021) Further insights of a composite implicit time integration scheme and its performance on linear seismic response analysis. *Eng Struct* 241:112490
18. Malakiyeh MM, Shojaee S, Hamzehei-Javaran S, Bathe KJ (2021) New insights into the β_1/β_2 -Bathe time integration scheme when L-stable. *Comput Struct* 245:106433
19. Li J, Zhao R, Yu K, Li X (2022) Directly self-starting higher-order implicit integration algorithms with flexible dissipation control for structural dynamics. *Comput Methods Appl Mech Eng* 389:114274
20. Hulbert GM, Chung J (1996) Explicit time integration algorithms for structural dynamics with optimal numerical dissipation. *Comput Methods Appl Mech Eng* 137:175–188
21. Noh G, Bathe KJ (2013) An explicit time integration scheme for the analysis of wave propagations. *Comput Struct* 129:178–193
22. Soares D (2016) A novel family of explicit time marching techniques for structural dynamics and wave propagation. *Comput Methods Appl Mech Eng* 311:838–855
23. Kim W (2019) A new family of two-stage explicit time integration methods with dissipation control capability for structural dynamics. *Eng Struct* 195:358–372
24. Soares D (2021) A novel single-step explicit time-marching procedure with improved dissipative, dispersive and stability properties. *Comput Methods Appl Mech Eng* 386:114077
25. Soares D (2021) A multi-level explicit time-marching procedure for structural dynamics and wave propagation models. *Comput Methods Appl Mech Eng* 375:113647
26. Wen W, Deng S, Duan S, Fang D (2021) A high-order accurate explicit time integration method based on cubic b-spline interpolation and weighted residual technique for structural dynamics. *Int J Numer Meth Eng* 122:431–454
27. Li J, Yu K, Zhao R (2022) Two third-order explicit integration algorithms with controllable numerical dissipation for second-order nonlinear dynamics. *Comput Methods Appl Mech Eng* 395:114945
28. Sofiste TV, Soares D, Mansur WJ (2020) An effective locally defined time marching procedure for structural dynamics. *Struct Eng Mech* 73:65–73
29. Soares D (2022) A novel conjoined space–time formulation for explicit analyses of dynamic models. *Engineering with Computers*. <https://doi.org/10.1007/s00366-021-01565-7>
30. Soares D (2022) An improved adaptive formulation for explicit analyses of wave propagation models considering locally-defined self-adjustable time-integration parameters. *Comput Methods Appl Mech Eng* 399:115324
31. Soares D (2015) A simple and effective new family of time marching procedures for dynamics. *Comput Methods Appl Mech Eng* 283:1138–1166
32. Soares D (2022) Two efficient time-marching explicit procedures considering spatially/temporally-defined adaptive time-integrators. *Int J Comput Methods* 19:2150051
33. Soares D, Pinto LR, Mansur WJ (2023) A truly-explicit time-marching formulation for elastodynamic analyses considering locally-adaptive time-integration parameters and time-step values. *Int J Solids Struct* 271–272:112260
34. Soares D (2023) An enhanced explicit-implicit time-marching formulation based on fully-adaptive time-integration parameters. *Comput Methods Appl Mech Eng* 403:115711
35. Soares D (2019) A model/solution-adaptive explicit-implicit time-marching technique for wave propagation analysis. *Int J Numer Meth Eng* 119:590–617
36. Dahlquist G (1963) A special stability problem for linear multistep methods. *BIT* 3:27–43
37. Batra RC, Porfiri M, Spinello D (2008) Free and forced vibrations of a segmented bar by a meshless local Petrov-Galerkin (MLPG) formulation. *Comput Mech* 41:473–491
38. Han S (2016) Finite volume solution of 2-D hyperbolic conduction in a heterogeneous medium. *Numer Heat Transfer Part A* 70:723–737

Publisher's Note Springer Nature remains neutral with regard to jurisdictional claims in published maps and institutional affiliations.

Springer Nature or its licensor (e.g. a society or other partner) holds exclusive rights to this article under a publishing agreement with the author(s) or other rightsholder(s); author self-archiving of the accepted manuscript version of this article is solely governed by the terms of such publishing agreement and applicable law.